Using a holographic imager on a tethered balloon system for microphysical observations of boundary layer clouds

Fabiola Ramelli[1], Alexander Beck[1], Jan Henneberger[1], and Ulrike Lohmann[1]

[1]Institute for Atmospheric and Climate Science, ETH Zurich, 8092 Zurich, Switzerland

Correspondence: Fabiola Ramelli (fabiola.ramelli@env.ethz.ch)
Jan Henneberger (jan.henneberger@env.ethz.ch)

Abstract. Conventional techniques to measure boundary layer clouds such as research ~~aircrafts~~ aircraft are unable to sample in ~~orographic or densely-populated~~ orographically diverse or densely populated areas. In this paper, we present a newly developed measurement platform on a tethered balloon system (HoloBalloon) to measure in situ vertical profiles of microphysical and meteorological cloud properties up to 1 kilometer above ground. The main component of the HoloBalloon platform is a holographic imager, which uses digital in-line holography to image an ensemble of cloud particles in ~~a velocity independent sample volume, making it~~ the size range from small cloud droplets to precipitation-sized particles in a three-dimensional volume. Based on a set of two-dimensional images, information about the phase-resolved particle size distribution, shape and spatial distribution can be obtained. The velocity-independent sample volume makes holographic imagers particularly well suited for measurements on a balloon. The unique combination of holography and balloon-borne measurements allows for observations with high spatial resolution, covering cloud structures from the kilometer down to the millimeter scale.

The potential of the measurement technique in studying boundary layer clouds is demonstrated on the basis of a case study. We present observations of a supercooled low stratus cloud ~~(high fog event)~~ during a Bise situation over the Swiss Plateau in February 2018. In situ microphysical profiles up to 700 m altitude above the ground ~~and~~ were performed at temperatures down to -8 °C and wind speeds up to 15 m s^{-1} ~~were performed~~. We were able to capture unique microphysical ~~features from the kilometer down to the meter scale. For example, we observed cloud regions with decreased cloud~~ signatures in stratus clouds, in the form of inhomogeneities in the cloud droplet number concentration ~~(<0.5 $\overline{CDNC}$)~~ and cloud droplet size~~at scales of 30-50 meters. These cloud inhomogeneities could arise from adiabatic compression and heating and subsequent droplet evaporation in descending air parcels. Moreover, we observed conditions favorable for the formation of boundary layer waves and Kelvin-Helmholtz instability at the cloud top. This potentially influenced the cloud structure on a scaleof 10-30 kilometers, which is reflected in the variability of the CDNC.~~ , from the kilometer down to the meter scale.

1 Introduction

Boundary layer clouds play a key role in regulating the Earth's climate~~and~~ , controlling its weather systems and are important for many aspects of our daily life. First, low-level clouds are an important part of the Earth's radiation balance (Hartmann et al., 1992). For example, low stratus clouds cover an extensive area over ocean and land (~~Warren et al. 1986, Warren et al. 1988~~

Warren et al., 1986; Warren et al., 1988), can persist for several days (e.g. ~~Bendix 2002~~Bendix, 2002) and cool the surface in the annual mean (e.g. ~~Randall et al. 1984~~Randall et al., 1984). Second, low visibilities associated with fog can impact road, ship and aviation traffic, causing accidents, delays or cancellations (e.g. ~~Fabbian et al. 2007, Bartok et al. 2012~~Fabbian et al., 2007 ; Bartok et al., 2012). The resulting economic losses are comparable to those caused by winter storms (Gultepe et al., 2007). Moreover, with the constantly increasing contribution of photovoltaic power, reliable forecasts of low-level cloud cover are of increasing importance for the renewable energy sector (Köhler et al., 2017).

However, current state-of-the-art numerical weather prediction (NWP) models have major issues in predicting the exact time and location of the formation and dissipation of low-level boundary layer clouds (e.g. ~~Bergot et al. 2007, Müller et al. 2010, Steeneveld et al. 2015, Román-Cascón et al. 2016~~Bergot et al., 2007; Müller et al., 2010; Steeneveld et al., 2015; Román-Cascón et al., 20). This is due to an incomplete understanding and a poor representation of the numerous processes occurring in boundary layer clouds, spanning from the microscale to the synoptic scale. The life cycle of boundary layer clouds is a result of complex interactions among microphysical, thermodynamic, radiative, dynamic, aerosol and land surface processes. These processes are often not well parameterized in current operational NWP models, and the horizontal (Pagowski et al., 2004) and vertical (Tardif, 2007) resolution of these models is insufficient to cover the characteristic cloud scales. From an observational perspective, there is a need for additional comprehensive and high-quality observations of boundary layer clouds, especially of their vertical structure. Presently, ~~most~~ a large fraction of the observations of boundary layer clouds ~~are~~ is performed by satellites ~~.~~ (e.g. Bendix, 2002; Bennartz, 2007; Cermak et al., 2009; van der Linden et al., 2015). Satellites have a continuous spatial coverage and are useful to obtain climatologies of the optical and microphysical properties of clouds (~~Bendix 2002, Cermak and Bendix 2008~~Bendix, 2002; Cermak et al., 2009). However, current satellite observations are typically too coarse to resolve scales below 250 m and have limitations in measuring cloud properties in the lowest kilometer of the planetary boundary layer (PBL) due to interference signals from the ground ~~.~~ (e.g. Marchand et al., 2008; Liu et al., 2017). Thus, in situ measurements of boundary layer clouds are important to gain a better understanding of the microphysical pathways in clouds. Commonly, microphysical in situ measurements within the PBL are performed using a variety of measurement platforms, such as research aircraft (e.g. ~~Sassen et al. 1999, Verlinde et al. 2007~~Sassen et al., 1999; Verlinde et al., 2007), helicopters (e.g. ~~Siebert et al. 2006~~Siebert et al., 2006), cable cars (e.g. ~~Beck et al. 2017~~Beck et al., 2017), tethered balloon systems (TBS) (e.g. ~~Siebert et al. 2003, Maletto et al. 2003, Lawson et al. 2011, Sikand et al. 2013, Canut et al. 2016~~Siebert et al., 2003; Maletto et al., 2003 ; Lawson et al., 2011; Sikand et al., 2013; Canut et al., 2016) or launched balloon platforms (e.g. ~~Creamean et al. 2018~~Creamean et al., 201), each of which has its own advantages and disadvantages. For example, research aircraft can travel large distances and freely choose their flight path, but have minimum altitude constraints, which limits observations within the lowest kilometer of the PBL. Moreover, due to high travelling speeds (100 $\mathrm{m\,s^{-1}}$), aircraft measurements have limited spatial resolution and can be influenced by ice shattering ~~on~~ (Korolev et al., 2011). Ice shattering occurs if an ice crystal impacts the instrument tips ~~(Korolev et al., 2011)~~or an inlet prior to entering the detection volume, which can result in a large number of small ice particles being a measurement artefact. To investigate small-scale processes in clouds, measurement platforms with lower true air speed are advantageous. The aspiration speed on cable cars (10 $\mathrm{m\,s^{-1}}$) is one order of magnitude lower than on ~~aircraft~~aircrafts, which enables probing the cloud with a much higher spatial resolution (Beck et al., 2017). However, the locations of cable cars

are limited to mountain areas. TBS can achieve a similar instrumental resolution as cable cars and are more flexible in terms of choosing the measurement location. Measurements with TBS can cover the full vertical extent of the PBL from the surface up to 1-2 kilometers. However, conventional, blimp-like TBS are limited to wind speeds below $10\,\mathrm{m\,s^{-1}}$ due to the instability of the balloon at higher wind speeds (e.g. ~~Lawson et al. 2011, Canut et al. 2016, Mazzola et al. 2016~~Lawson et al., 2011; Canut et al., 2016; Mazzola et al., 2016). Moreover, TBS can be deployed further away from the ground, reducing the effects of surface-based processes such as blowing snow (~~Lloyd et al. 2015, Beck et al. 2018~~Lloyd et al., 2015; Beck et al., 2018).

In this paper, we present a newly developed measurement platform for boundary layer clouds (HoloBalloon), consisting of a holographic cloud imager and a meteorological instrument package on a kytoon. Kytoons are a hybrid-balloon-kite combination allowing stable flight in wind speeds up to $30\,\mathrm{m\,s^{-1}}$. The stability in high wind speeds makes kytoons a promising measurement platform for cloud research, especially in locations with strong wind conditions (e.g. mountain regions). Due to the low aspiration velocities of TBS, the choice of the instrument is of particular importance, since fluctuations in wind speed and direction could influence the measurements. Most cloud probes use an inlet to ensure a steady sampling velocity in fluctuating wind speeds (Baumgardner et al., 2011). However, the use of inlets increases measurement uncertainty, due to size-dependent particle losses at the inlet and non-isokinetic sampling effects. One technique that overcomes this problem is digital in-line holography, which provides a well-defined sample volume independent of particle size and aspiration velocity, making holographic cloud imagers particularly well suited for measurements on TBS. Digital in-line holography can simultaneously capture single particle information (position, size and shape) of an ensemble of cloud particles within a three-dimensional detection volume. Thus, it provides information of the phase-resolved ~~cloud properties such as number concentration, size distribution , and water content~~ particle size distribution (e.g. ~~Beck et al. 2017~~Beck et al., 2017), as well as the spatial distribution of ~~cloud particles in~~ an ensemble of cloud particles within a cloud volume on a millimeter scale (e.g. ~~Beals et al. 2015).~~ Beals et al., 2015). More detailed information about the working principle of a holographic imager will follow in Sect. 3.1. Digital holographic cloud imagers have been used in previous field campaigns on ground-based (e.g. ~~Thompson 1974, Kozikowska et al. 1984, Borrmann et al. 1993, Raupach et al. 2006, Henneberger et al. 2013, Schlenczek et al. 2017~~Thompson, 1974; Kozikowska et al., 1984 ; Borrmann et al., 1993; Raupach et al., 2006; Henneberger et al., 2013; Schlenczek et al., 2017), airborne (e.g. ~~Conway et al. 1982 , Fugal and Shaw 2009, Beals et al. 2015, Glienke et al. 2017~~Conway et al., 1982; Fugal and Shaw, 2009; Beals et al., 2015; Glienke et al., 2017; Desai et al., 2019) and cable car (Beck et al., 2017) platforms, but have not yet been deployed on TBS.

The HoloBalloon platform merges the advantages of holography (well-defined sampling volume, spatial distribution of cloud particles) with the benefits of a TBS (high-resolution measurements) with the aim to observe the cloud structure on different scales. Information about the macroscopic cloud structure can be obtained from the vertical profiles up to 1 kilometer above the ground and information about the cloud microstructure can be extracted from the ~~analysis of the~~ cloud particle spatial distribution within a single hologram~~on a millimeter scale~~. The HoloBalloon platform was tested in boundary layer clouds over the Swiss Plateau. Here we present observations of a case study during a stratus cloud ~~(high fog)~~ event. The cloud structure is analyzed on different scales, starting with the large-scale cloud structure of tens of kilometers and moving down to the cloud microstructure on the meter scale. A particular emphasis is placed on cloud inhomogeneities. Previous observations found ~~microphysical inhomogeneities~~ inhomogeneities in cloud properties on scales of a few tens of meters (e.g.

Korolev and Mazin 1993, Garcıa-Garcıa et al. 2002, Gerber et al. 2005Korolev and Mazin, 1993; Garcıa-Garcıa et al., 2002; Gerber et al.,) or even on the sub-meter scale (e.g. Baker 1992, Brenguier 1993, Beals et al. 2015, Beck et al. 2017Baker, 1992; Brenguier, 1993 ; Beals et al., 2015; Beck et al., 2017; Desai et al., 2019), which were attributed to different physical processes such as turbulent mixing or entrainment. These inhomogeneities can influence the cloud microphysics on different scalesmicrophysical signatures can have important implications for the cloud structure. For example, on a millimeter scale, they can be of importance for particle growth by collision-coalescence and thus for the efficiency of precipitation formation. Inhomogeneities at scales of hundreds of meters and kilometers can be important for radiative heating and cooling. In this paper, we investigate whether similar cloud inhomogeneities are found in inhomogeneities in the microphysical properties of stratus clouds and aim to understand the formation mechanisms of such inhomogeneities. Throughout this study, inhomogeneities are defined by the variability in the cloud droplet number concentration and cloud droplet size.

The first part of the paper introduces the HoloBalloon measurement platform (Sect. 2). The working principle and the setup of the newly developed holographic cloud imager is described in Sect. 3. Observations of a case study in stratus clouds during a Bise situation obtained with HoloBalloon are presented in Sect. 4. These observationsare discussed in a larger context in On the basis of these observations, the potential of the HoloBalloon platform in studying boundary layer clouds is discussed in Sect. 5.

2 Description of the HoloBalloon measurement platform

The HoloBalloon platform is designed to obtain vertical, in situ profiles of the microphysical and meteorological cloud properties of boundary layer clouds up to 1 kilometer above ground. Our TBS consists of a 175 m^3 kytoon (Desert Star, Allsopp Helikite, UK), a 1200 m long Dyneema cable and a gasoline winch to launch and recover the TBS (see Fig. 1). The balloon has a net lift of 85 kg at sea level. Kytoons are a hybrid combination of a helium balloon and a kite, exploiting both for lift. The helium balloon creates static lift, while the kite creates aerodynamic lift in wind. The kite utilizes a long keel to provide stability in high wind conditions. The maximum operational wind speed of our TBS is 25 $m\,s^{-1}$. So far, we operated the TBS in wind speeds of up to 15 $m\,s^{-1}$. A further advantage of the kite is that it ensures that the instrument platform is oriented into the wind, allowing for the spatial distribution of cloud particles to be assessed.

The cable and winch are designed to withstand forces up to 4 tons, which can occur during high wind speed conditions ($> 15\,m\,s^{-1}$). The 7 mm Dyneema line cable has a length of 1200 m and a breaking strength of 8200 kg. At wind speeds larger than 5 $m\,s^{-1}$, the TBS can have a flight angle of up to 45° due to the kytoon design, reducing the maximum flight height to 850 m. A system of three Platipus anchors is used to secure the balloon to the ground. The tethered balloon is launched and retrieved with a winch powered by a V8 Chevy engine (Skylaunch, UK). The winch has a line speed of 1 $m\,s^{-1}$ forward and reverse, which allows a vertical profile of 500 m in 8 minutes.

The instrument package is installed at the kiel keel of the HoloBalloon platform. The key component is the HOLographic Imager for Microscopic Objects (HOLIMO 3B) (see Sect. 3) which can measure phase-resolved cloud properties. Additionally, the HoloBalloon platform is equipped with a meteorological instrument package (see Fig. 1) consisting of a 3D sonic

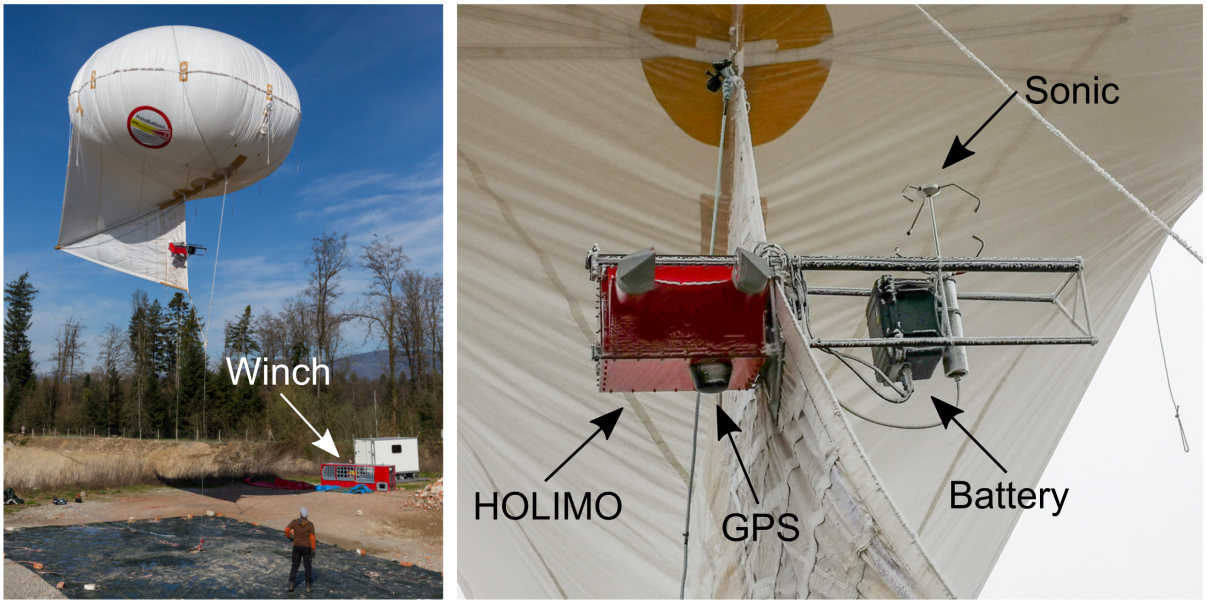

Figure 1. Experimental setup of the HoloBalloon platform consisting of a tethered balloon system (left) and the instrument package (right). The winch is visible in the left picture. The instrument package includes the holographic cloud imager HOLIMO 3B, a 3D sonic anemometer as well as a temperature and humidity sensor (not visible). The left picture has been taken by Pascal Halder (naturphotos.ch)

anemometer (THIES, 4.3830.20.340) and a heated temperature and humidity sensor (HygroMet4, Rotronic) in an actively ventilated radiation shield (RS24T, Rotronic). The platform is powered by a 1000 Wh battery, which allows for continuous operation of the instrument package for up to 5 hours. Data are temporally stored on a 4 TB solid state drive and a mobile router enables remote access of the platform via a mobile data network connection (similar to ~~Beck et al. 2017~~Beck et al., 2017). The HoloBalloon instrument platform has a total weight of about 22 kg, consisting of the HOLIMO 3B instrument (13 kg), the meteorological instrumentation (5 kg) and the battery pack (4 kg).

To obtain reliable measurements of wind speed and direction the motion of the balloon needs to be removed (e.g. ~~Canut et al. 2016~~ Canut et al., 2016). Here we used a GPS antenna (TW3740, Tallysman) and an inertial navigation system (Ellipse2-N, SBG systems) to measure the position, velocity and orientation of the instrument package. The GPS antenna and the inertial navigation system are fixed on the HOLIMO 3B instrument and are thus an integral part of the instrument package. We followed the procedure described in Elston et al. (2015) to convert the wind measurements from the inertial frame to the sonic anemometer frame and thus to correct for the motion of the balloon. The corrected wind measurements are presented and compared to other wind observations in Sect. 4.2.

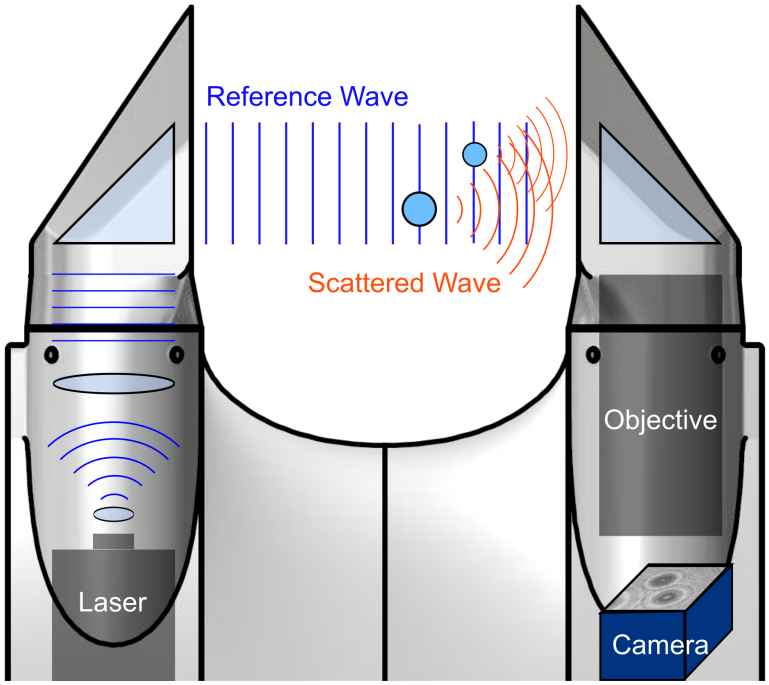

Figure 2. Schematic of the working principle of digital in-line holography. A collimated laser beam is scattered by two particles. The scattered waves interfere with the reference wave and form an interference pattern (i.e. a hologram) which is recorded by a digital camera.

3 HOLographic Imager for Microscopic Objects

The main component of the HoloBalloon instrument package is the holographic cloud imager HOLIMO 3B, which can image cloud particles between 6 µm and 2 mm within a three-dimensional detection volume. Despite its open path configuration, HOLIMO~~has a velocity independent~~ 3B has a velocity-independent well-defined sample volume. This property makes HOLIMO 3B particularly well suited for application on a TBS due to fluctuating aspiration speeds towards a TBS.

3.1 Working principle of digital in-line holography

HOLIMO 3B works on the principle of digital in-line holography (Fig. 2), which consists of a two-step process requiring a coherent light source and a digital camera. In the first step, the interference pattern of a reference wave (laser) and a scattered wave (the light scattered by a cloud particle in the sample volume) is recorded as a hologram. The second step involves a reconstruction process, in which the 2D shadowgraphs and 3D in-focus position of the particles are extracted from the interference pattern, using the HoloSuite software package (~~Fugal et al. 2009, Schlenczek 2018~~Fugal et al., 2009; Schlenczek, 2018). The resulting 2D shadowgraphs can be classified as cloud droplets, ice crystals and ~~artifacts~~ artefacts based on a set of parameters using supervised machine learning (e.g. ~~Fugal et al. 2009, Beck et al. 2017, Touloupas et al. 2019 (submitted). From that, we can calculate~~ Fugal et al., 2009; Beck et al., 2017; Touloupas et al., 2019). In the present study, a set of around 7000 particles

was classified manually, which served as a training data set on support vector machines. From the classification, the phase-resolved ~~microphysical properties such as number concentration, water content and size distribution~~particle size distribution is computed. The particle diameter is calculated based on the number of pixels (see also Sect. 3.3) and the number concentration can be computed from the particle counts within the well-defined sample volume. Only particles that exceed a size of 2×2 pixels (6 µm) are considered. Moreover, because holography provides a snapshot of an ensemble of cloud particles~~within a volume~~, the spatial distribution of the cloud particles can be recovered from the interference pattern. Unlike light scattering instrumentation, no assumptions about the particle shape, orientation or refractive index are required, ~~as~~ because an image of the cloud particles is ~~captured~~recorded. The major disadvanted of holography is the high computational power associated with the reconstruction process and the data analysis. The working principle of digital in-line holography and HOLIMO ~~have~~ has been described in more detail in Fugal et al. (2009), Henneberger et al. (2013) and Beck et al. (2017).

3.2 Instrument description

A series of holographic instruments have been developed in the Atmospheric Physics group at ETH Zurich in the last decade (~~Amsler et al. 2009, Henneberger et al. 2013, Beck et al. 2017~~Amsler et al., 2009; Henneberger et al., 2013; Beck et al., 2017). HOLIMO 3B consists of two main units: The control unit, which comprises the temperature control system and the control and data-acquisition computer, and the optical imaging unit, which is integrated in the two instrument towers. As the previous version (HOLIMO 3G, ~~Beck et al. 2017~~Beck et al., 2017), HOLIMO 3B has an open path configuration. In contrast to the previous versions, HOLIMO 3B uses a 355 nm laser and an improved optical system to enlarge the detection volume and improve the optical resolution of the instrument.

A schematic of the optical system of HOLIMO 3B is shown in Fig. 2. The laser (FTSS355-Q4_1k, CryLas, Germany) emits pulses with a wavelength of 355 nm, with a pulse width of 1.4 ns and a pulse energy of 42 µJ. The beam is attenuated by a neutral density filter and focused through a 10 µm diamond pinhole (LenoxLaser HP-3/8-DISC-DIM-10), which acts as a point light source. The diverging laser beam is expanded by a biconcave lens and collimated to a beam diameter of around 40 mm. After passing through a turning prism and a sapphire window, the collimated laser beam traverses the sample volume, before entering the imaging lens system in the opposite tower of the instrument. The bi-telecentric lens system (Correctal S5LPJ2755, TDL65/1.5 UV, Sill Optics, Germany) has a magnification of 1.5 and a numerical aperture of 0.13. The holograms are recorded with a 25 MP camera (hr25000MCX, SVS-Vistek, Germany) with 5120×5120 pixels, a pixel pitch of 4.5 µm and a maximum frame rate of 80 fps. The quadratic cross-sectional area of the camera allows for more uniform illumination of the edges than a rectangular camera image, which was used in the previous versions.

The optical resolution of the system was tested using a US Air Force resolution target (1951 USAF), which is placed at different positions inside the detection volume, following the procedure described in Spuler and Fugal (2011) and Beck et al. (2017). The optical system described achieves a resolution ($D_{res,obs}$) of 6 µm within the first 110 mm of the reconstruction distance (see Fig. 3). This is consistent with the theoretical resolution limit of the pixel size ($D_{res,pixel}$). For reconstruction distances larger than 110 mm, the resolution limit decreases and is determined by the resolution limit from the diffraction aspects of in-line holography ($D_{res,rec}$). In general, the measured optical resolutions are in good agreement with the theoretical

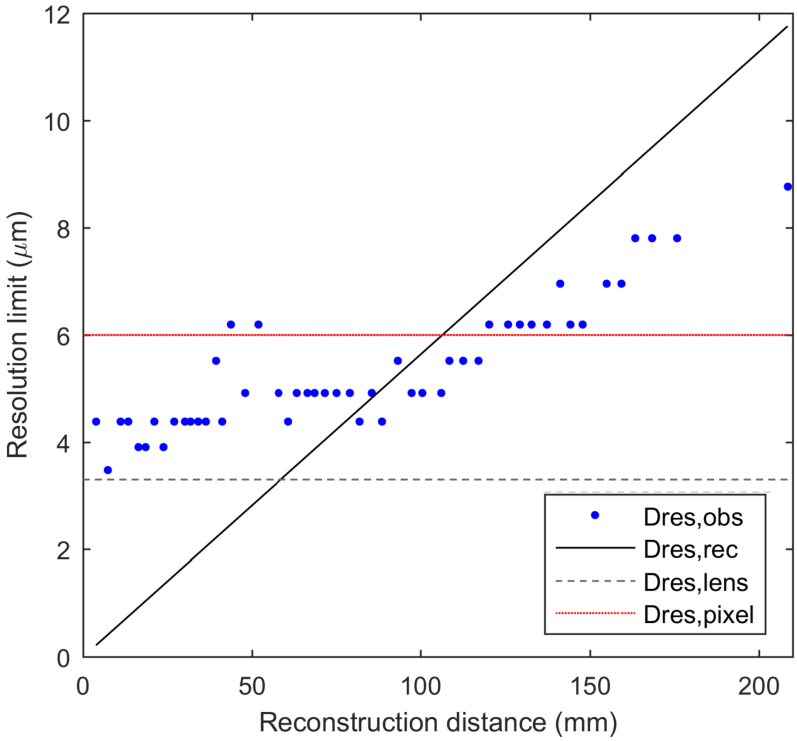

Figure 3. Optical resolution measurements of the HOLIMO 3B instrument as a function of the reconstruction distance. The blue dots represent the resolutions measured with a US Air Force resolution target 1951 USAF ($D_{res,obs}$). The three lines indicate theoretical resolution limits due to the pixel size ($D_{res,pixel}$, red solid line), the optical limitation of the lens system ($D_{res,lens}$, grey dashed line) and the optical setup of the instrument ($D_{res,rec}$, black solid line). The strongest resolution limit constraint determines the optical resolution of the instrument at a specific reconstruction distance. More information about the theoretical resolution constraints for holographic systems can be found in Henneberger et al. (2013) and Beck et al. (2017).

resolution constraints. Particles within the first 10 mm and close to the image border (< 0.2 mm from image edges) are not included in the analysis due to flow distortion effects from the towers and edge effects. With an effective cross-sectional area of 15 mm × 15 mm and an effective depth of 100 mm, this results in a sample volume of 22.5 cm^3 and a maximum sample volume rate of 1800 $cm^3 s^{-1}$ (with 80 fps).

3.3 Size calibration of HOLIMO 3B

Accurate sizing of cloud particles is important to obtain reliable measurements of cloud properties such as water content and size distributions. For holographic instruments, the sizing algorithm should be precise and accurate over a large particle size range (6 µm - 1 cm) and applicable for the entire detection volume. The sizing of the particles strongly depends on an amplitude threshold value that separates particle pixels from background pixels. From the number of particle pixels, the area-equivalent

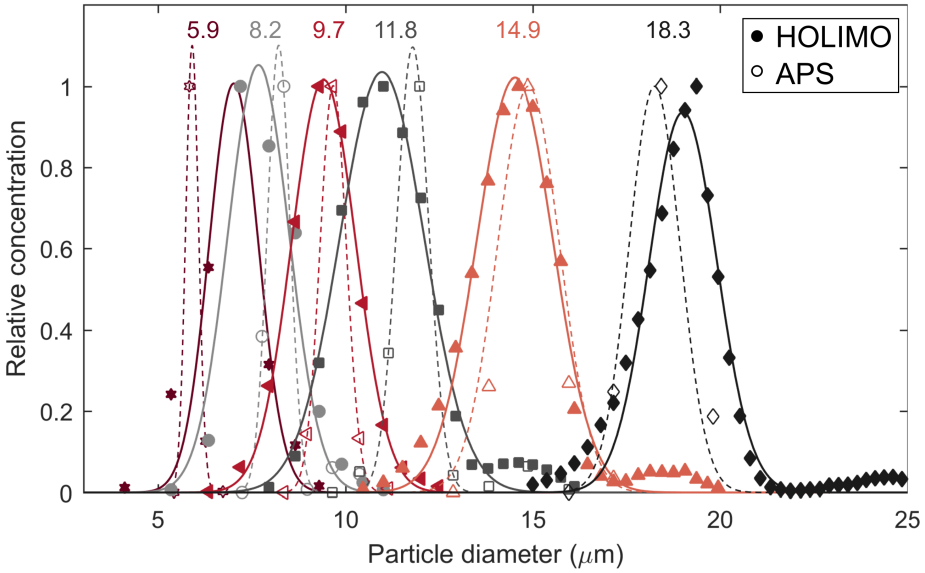

Figure 4. Size distributions from calibration experiments of the HOLIMO 3B instrument. The symbols show the normalized particle concentration measured by HOLIMO 3B (filled) and the APS (unfilled) instrument. The lines indicate the Gaussian distributions fitted to the HOLIMO 3B data (solid) and APS data (dashed). The numbers represent the mean diameter of the APS size distribution.

diameter is derived. In the standard HoloSuite version, a uniform amplitude threshold is used for particle detection and particle sizing. However, a uniform amplitude threshold leads to unsatisfying results for particle sizing due to a decreasing signal-to-noise ratio with increasing reconstruction distance z in the large detection volume of HOLIMO 3B. This has the effect that the amplitude image of the particles becomes less distinct with larger z distances and thus the observed particle size decreases with increasing z distance. To overcome this issue and to ensure a uniform sizing of the particles over the entire detection volume, Beck (2017) introduced a new method by normalizing the in-focus particle image. In the normalization step, the darkest particle pixel is set to 0 (black), the mean of the background pixels is set to 1 (white) and the rest of the pixels are scaled relatively. This results in a more uniform signal-to-noise ratio and allows applying a uniform amplitude threshold. The amplitude threshold can be used as a tuning parameter to calibrate the sizing algorithm of the HoloSuite software for the HOLIMO 3B instrument. The sizing algorithm was calibrated using a Vibrating Orifice Aerosol Generator (VOAG model 3450, TSI, Minnesota, USA) for particle generation and an Aerodynamic Particle Sizer (APS model 3321, TSI, Minnesota, USA) for particle sizing. Particles with diameters between 5 µm and 18 µm were generated by the VOAG using a liquid oil-water solution. The generated particles were introduced into a 120 mm × 1000 mm cylindrical tube and measured by the HOLIMO 3B instrument and an APS that were installed at the end of the tube. The APS covers the size range between 1 µm and 20 µm and is used as a reference measurement. ~~Thus, the~~ The amplitude threshold was used as a tuning parameter to fit the HOLIMO 3B measurements to the APS measurements. An amplitude threshold of 0.47 was found to fit the APS data best (smallest sum of squared errors).

The size distributions of the calibration experiments are shown in Fig. 4 and are summarized in Table 1. The size distributions

of the HOLIMO 3B and APS instruments were normalized to their maxima and a Gaussian distribution was fitted to the data. The results of the HOLIMO 3B instrument agree with the mean diameter of the APS within instrumental uncertainty. In general, a trend towards an underestimation of the particle diameter compared to the APS is observed, except for the calibration measurements at the measurement limits of HOLIMO 3B (6 µm) and the APS (18 µm). The overestimation of the particle diameter by HOLIMO 3B for 6 µm particles may be due to the optical resolution limit of the HOLIMO 3B instrument. While HOLIMO 3B can only detect particles larger than 6 µm, the APS can detect particles down to a diameter of 1 µm. On the other hand, the overestimation of the particle diameter at 18 µm could be caused by a bias of the APS instrument, which has an upper detection limit of 20 µm. Thus, particles in the second peak at 23 µm are not detected by the APS (see Fig. 4). To conclude, no correction to the sizing algorithm was made, because all size measurements agree within the square root of the pixel size ($\sqrt{3.01\ \mu m} = 1.73\ \mu m$).

4 Case study - Supercooled low stratus clouds

~~In this paper~~As a case study, we present observations of a supercooled low stratus cloud event (also referred to as high fog) during a Bise situation over the Swiss Plateau, obtained on 24 February 2018 between 08 and 10 UTC. Bise is a typical weather situation in Switzerland during winter (Wanner and Furger, 1990). The case study focuses on 9 vertical profiles of microphysical and meteorological cloud properties measured by the HoloBalloon platform. The analysis starts ~~with large scales, giving~~ with an overview of the synoptic weather situation and the large-scale cloud structure, and moves towards smaller scales, providing information about the cloud microstructure.

The Swiss Plateau, which lies between the Jura mountains and the Swiss Alps, is often covered by fog or low stratus clouds during autumn and winter due to its geographic location. A satellite-based climatology of fog and low stratus cloud coverage over the Swiss Plateau during high pressure situations in winter is shown in Fig. 5. In regions along rivers and lakes, a fog frequency of up to 90 % is observed. Most commonly, fog forms by radiative cooling during clear nights. Additionally, cold air flows from the alpine valleys and the Jura towards the Swiss Plateau, where the cold air can accumulate. This cooling of the air can cause condensation and the formation of ground fog. However, the case study presented here was connected to a Bise situation; a cold, dry east~~and~~ / north-east wind. During Bise, cold air is advected and pushed under warm air, leading to the formation of a strong temperature inversion. The cold air in the lower layer cannot easily escape the Swiss Plateau because

Table 1. Results of the size calibration experiments of HOLIMO 3B and an APS. The mean diameter and the standard deviation are derived from a Gaussian fit to the normalized size distribution.

	Particle diameter (µm)					
HOLIMO 3B	7.02 ± 0.93	7.68 ± 1.15	9.41 ± 1.21	10.97 ± 1.59	14.52 ± 1.45	19.01 ± 1.28
APS	5.91 ± 0.24	8.21 ± 0.42	9.67 ± 0.50	11.79 ± 0.60	14.88 ± 1.18	18.25 ± 0.96

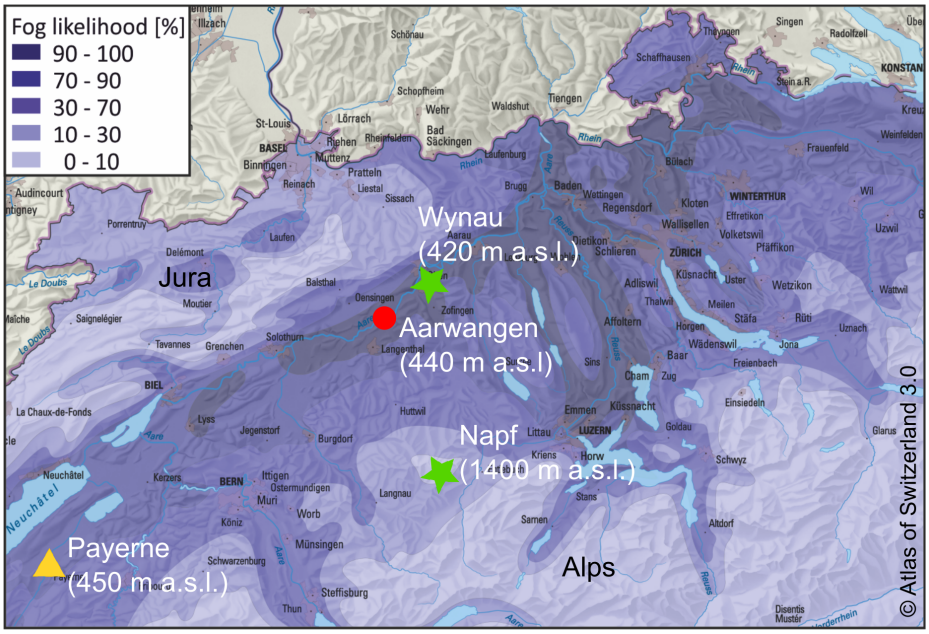

Figure 5. Map of the fog frequency during winter (adapted from the 'Atlas of Switzerland 3.0', 2010, https://www.atlasderschweiz.ch/) and of the measurement locations. The climatology of fog is based on satellite images. The field locations ~~comprise~~ include the measurement site in Aarwangen from which HoloBalloon was launched (red circle), ground-based weather stations from MeteoSwiss providing measurements of meteorological parameters (green stars) and the field site in Payerne from which radiosondes are launched twice a day (yellow triangle).

it is bound by the Jura mountains and the Swiss Alps. If the air is sufficiently moist, condensation sets in and ~~high~~ fog or low stratus clouds can develop. The top of the cloud layer is defined by the height of the temperature inversion. The solar radiation reaching the boundary layer is often too weak to dissipate the fog layer in autumn and winter. Thus, ground fog or stratus clouds can persist for several days, until a change in the synoptic weather pattern occurs.

4.1 Measurement location and data analysis

The measurements with the HoloBalloon platform were performed in Aarwangen (47°14' N, 7°45' E) in the Swiss Plateau 40 km northeast of Bern (Fig. 5). The field site is located at a gravel station next to the Aare river at an altitude of 440 m a.s.l. and is surrounded by grassland and forests. The balloon measurements were performed in a temporarily closed air space of 2 km in diameter, which was activated on measurement days. The maximum flight height allowed was 700 m above ground because of air traffic regulations. The experimental setup of the HoloBalloon platform is shown in Fig. 1.

The measurements taken on the HoloBalloon platform were complemented and validated by observations of surrounding MeteoSwiss weather stations and radiosondes (see Fig. 5). The weather stations are located within a radius of 30 km from Aarwangen and cover altitudes between 420 m a.s.l. and 1400 m a.s.l. ~~to obtain an overview of the regional weather situation.~~ Radiosondes are launched twice a day (00 and 12 UTC) from Payerne, which is located 80 km south-west of Aarwangen. We

Table 2. Summary of the start and end time of the 9 vertical profiles ~~taken~~ observed with the HoloBalloon platform.

Profile number	Profile type	Start time (UTC)	End time (UTC)
1	ascending	08:01	08:10
2	descending	08:11	08:23
3	ascending	08:24	08:34
4	descending	08:35	08:45
5	ascending	08:46	08:58
6	descending	08:59	09:11
7	ascending	09:12	09:22
8	descending	09:23	09:37
9	ascending	09:38	09:57

used the radiosondes to determine the inversion ~~height and thus the~~ and cloud top height, because we were not able to measure the whole cloud layer due to the air traffic restrictions on flight height.

A total of 9~~microphysical~~ vertical profiles measured with the HoloBalloon platform ~~was~~ were analyzed in this case study, with an average of 800 holograms (~5 L sampled volume) or 600'000 cloud particles per profile. The battery of the instrument package was empty after profile 9, thus no observations were available afterwards. Each profile had a duration of 10-15 minutes. With a mean horizontal wind speed of 10 m s^{-1}, this results in a horizontal resolution of around 6-9 kilometers. The start and end times of the individual profiles are summarized in Table 2. At least 10 holograms were grouped together to obtain better counting statistics. This results in a vertical resolution of 5 m. Only data points with a liquid water content (LWC) larger than 0.01 g m^{-3} (definition for cloud base) are considered in the analysis. Cloud particles smaller than 25 µm were classified into the three categories of cloud droplets, ice crystals and artefacts using support vector machines (see Sect. 3.1), whereas particles larger than 25 µm were classified ~~by hand~~manually (visual classification). Only particles within a reconstruction distance between 20 mm and 50 mm were included in the analysis. A smaller detection volume than described in Sect. 3.2 was chosen due to ~~a~~ the mean droplet size being close to the instrumental resolution limit and noise in the holograms.

4.2 Meteorological situation

Figure~~6 shows the~~ 6 shows vertical profiles of the meteorological parameters during the measurement period. The meteorological conditions during the 2-hour measurement period were relatively stable. The temperature profile was characterized by a strong temperature inversion, which was located at around 1450 m a.s.l. The temperature varied between -1 °C at the surface and -8.9 °C at the inversion base. The height of the temperature inversion defines the top of the cloud layer. The relative humidity increased from the ground up to 850 m a.s.l., where it remained constant up to the inversion. We assumed that this constant relative humidity interval indicates conditions of water saturation and thus marks the extent of the cloud layer. No relative

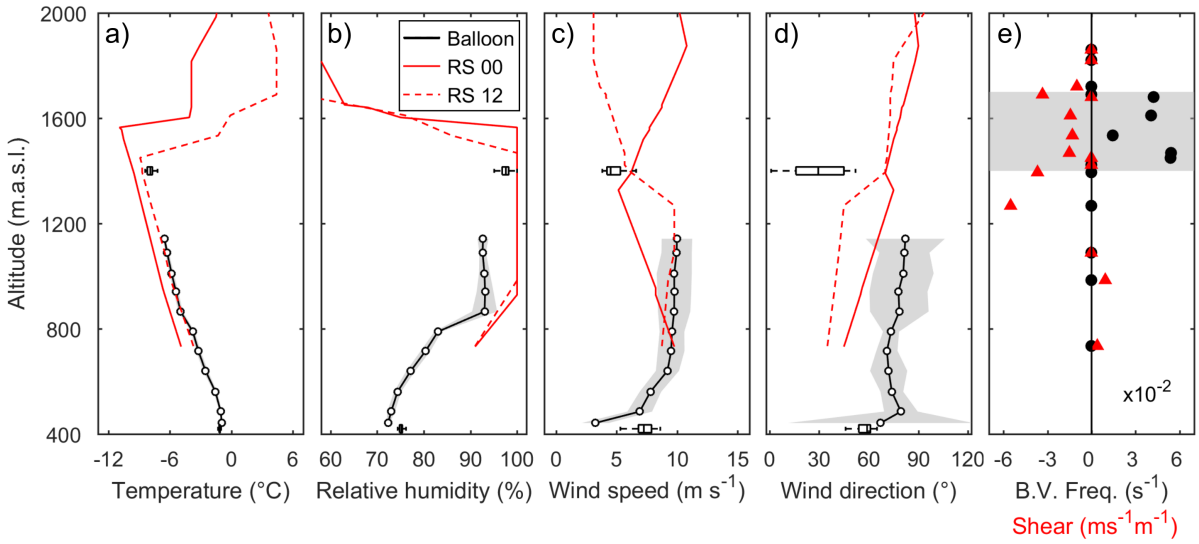

Figure 6. Vertical profiles of the meteorological parameters (a-d). The HoloBalloon measurements are averaged over 9 profiles and an altitude interval of 75 m. The black dots indicate the mean and the shaded area the standard deviation of the data. The vertical profiles of two radiosonde ascents (00 UTC (solid) and 12 UTC (dashed)) are shown by the red lines. The box plots represent the data from MeteoSwiss weather stations (Wynau (420 m a.s.l.), Napf (1400 m a.s.l.)). On each box, the central line indicates the median and the left and right edges of the box mark the 25th and 75th percentiles, respectively. The whiskers extend to the minimum and maximum of the data not considered as outliers. Figure ~~6c~~ 6.e shows the vertical profile of the Brunt-Väisälä frequency ($N = \sqrt{\frac{g}{\theta}\frac{\delta\theta}{\delta z}}$) and the wind shear ($s = \frac{\delta v}{\delta z}$) calculated from the radiosonde ascent at 12 UTC. The shaded area in Fig. 6.e indicates regions with a positive Brunt-Väisälä frequency.

humidity values above 95 % were observed by the HoloBalloon platform. This can be explained by the challenges of measuring relative humidity at in-cloud conditions (e.g. ~~Korolev and Mazin 2003, Korolev and Isaac 2006~~Korolev and Mazin, 2003 ; Korolev and Isaac, 2006). Wind speeds between 6.7 m s^{-1} and 8.6 m s^{-1} were observed in Wynau with wind gusts up to 10.6 m s^{-1}. The wind speed in Aarwangen increased in the first 200 m above the ground from 7 m s^{-1} to 10 m s^{-1}. As it can be seen from the radiosondes, the wind speed was relatively constant up to the inversion layer. The prevailing wind direction was north-east with a slight turn towards east with increasing altitude. At the inversion, a change in the horizontal wind speed and direction with height (vertical wind shear) occurs. In this region, a positive Brunt-Väisälä frequency N is observed (Fig. 6.e). These conditions are favorable for the development of boundary layer waves and Kelvin-Helmholtz instability (see Sect. 4.4). ~~With a Brunt-Väisälä frequency N of 0.04 s^{-1}, the period of oscillation is $\tau = 2\pi/N$ = 2.5 min, which lies in the range of typical wave periods of gravity waves in the boundary layer (few minutes up to one hour, Rees et al. 2000).~~

4.3 Microphysical cloud structure

Figure 7 shows the mean vertical profiles of the microphysical cloud properties averaged over 9 profiles. The mean cloud droplet number concentration (CDNC) increases from 10 cm^{-3} at the cloud base (920 m) to 150 cm^{-3} at 1100 m (Fig. 7.a).

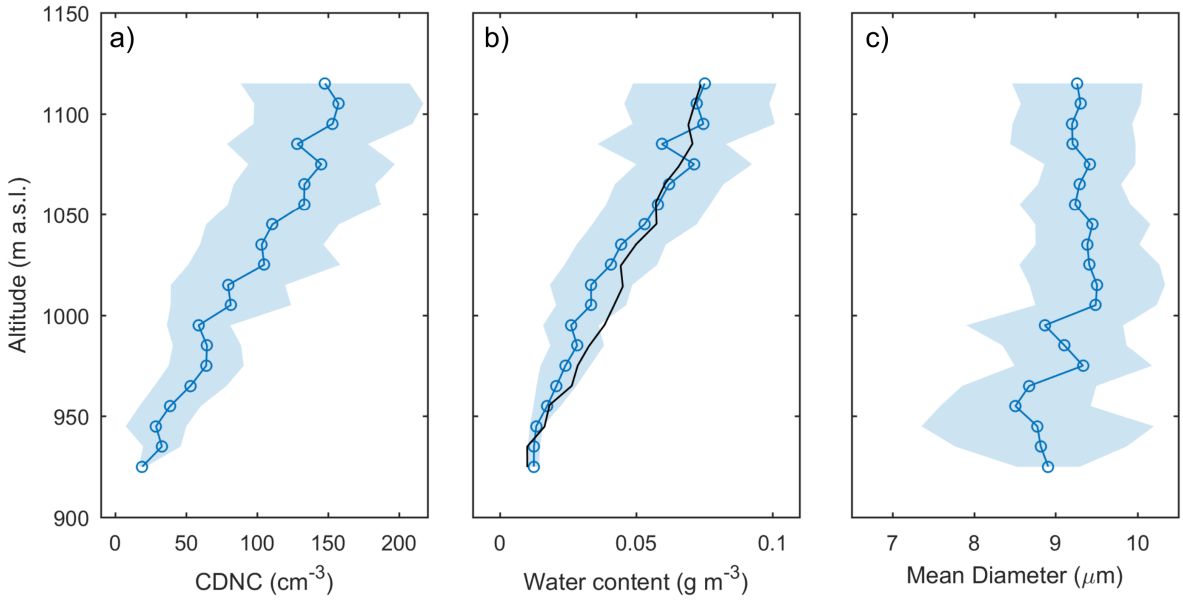

Figure 7. Mean vertical profiles of the cloud droplet number concentration (left), liquid water content (center) and mean cloud droplet diameter (right) averaged over the 9 profiles measured with the HoloBalloon platform. The data are averaged over an altitude interval of 10 m. The shaded area represents the standard deviation. The black line in b) shows the adiabatic LWC profile w_{l_ad}, which is ~~calculated~~ obtained as follows: i) calculate the saturation vapor pressure e_s at the cloud base, ii) use the pressure at the cloud base to determine the saturation mixing ratio $w_s(T,p) = \frac{\epsilon e_s(T)}{p-e_s}$, iii) calculate $w_t = w_s + w_l$ at the cloud base assuming $w_l = 0.01$ g kg^{-1} and assuming constant w_t with height (adiabatic), iv) calculate w_s at all height levels, determine w_l and multiply w_l by local dry air density to obtain w_{l_ad}.

The mean liquid water content (LWC) ranges between 0.01 gm^{-3} and 0.08 gm^{-3} and on average approaches an adiabatic profile (Fig. 7.b). The mean cloud droplet diameter ~~decreases slightly~~ increases from 9 µm to ~~8.5~~9.5 µm ~~in the first 30~~between the cloud base and 1000 m and stays constant ~~at around 9.5 m above 1000 m~~ above (Fig. 7.c). ~~The variability in the mean diameter is larger close to the cloud base. The~~ The observed CDNC of 150 cm^{-3}, LWC of 0.08 gm^{-3} and mean cloud droplet diameter of 9.5 µm are in the observed range for fog and continental stratus clouds (Lohmann et al., 2016), but rather at the lower end of the range. Despite the supercooled conditions, only a few ice crystals were observed (< ~~0.1~~1 L^{-1}).

The increase in CDNC with increasing height is in contrast to the theory of an adiabatic cloud profile and might be explained by different factors. An adiabatic cloud model assumes that cloud droplets activate at the cloud base and grow in size with increasing altitude. Thus, CDNC is expected to remain constant with height after the maximum supersaturation is reached. There are several possibilities why this theoretical ~~criterion is not met~~ concept is not applicable for the case study presented here. Firstly, HOLIMO 3B does not detect cloud droplets smaller than 6 µm. This can lead to an underestimation in CDNC, especially at cloud base where the droplets are the smallest. Secondly, an adiabatic cloud model assumes a constant updraft, but fluctuations in the updraft speed or turbulence could generate supersaturated conditions and activate cloud droplets at

higher altitudes than cloud base. Thirdly, the increase in CDNC with height could be driven by radiative cooling at the cloud top by producing either supersaturation and/or instabilities and thus turbulences within the cloud layer. ~~Moreover, it has to be considered that only the first 200 meters of the cloud were observed (up to 1150 m a.s.l), whereas the cloud top extends up to 1500 m a.s.l.~~ On the other hand, a database of stratus clouds (Miles et al., 2000) showed that the CDNC in continental clouds was more variable with height than in marine clouds where CDNC was determined near cloud base. ~~They suggested that different microphysical and dynamical processes occur in continental clouds, which could lead to a deviation of the theoretical assumption of a constant CDNC.~~ Therefore, it is unclear whether the observed increase in CDNC is a measurement artefact or a real feature of the observed cloud. Regardless, we recommend that future balloon-borne measurements of clouds include instruments capable of measuring even the smallest cloud particles.

4.4 Inhomogeneities in the microphysical cloud properties of stratus clouds

~~We~~ Upon further analysis, we investigate cloud inhomogeneities ~~by analyzing the height-temporal evolution of CDNCand of the anomaly of~~ in stratus clouds on different scales and discuss potential physical processes, which could influence these cloud signatures. In the present study, cloud inhomogeneities are defined by the variability in the CDNC. Therefore, we introduce the term CDNC anomaly ($CDNC_h^a$), which describes the variability of the CDNC over a given height interval h. The CDNC~~(Fig. 8). The CDNCanomaly CDNC$_h^a$~~ $_h^a$ is calculated by dividing the CDNC observed in the height interval h ($\overline{CDNC_h}$) by the mean CDNC in that height interval averaged over the 9 profiles ($\overline{CDNC_h}$) (i.e. $CDNC_h^a = CDNC_h/\overline{CDNC_h}$). ~~CDNC$_h^a$ reveals areas of higher and lower CDNC than the average concentration and gives indications of the CDNC variability within the cloud.~~ As Korolev and Mazin (1993), we define areas with $CDNC_h^a < 0.5$ as regions of decreased CDNC and areas with $CDNC_h^a > 1.5$ as regions of increased CDNC.

The height-temporal ~~evolution of~~ evolutions of the CDNC and $CDNC_h^a$ are shown in Fig. 8. CDNC~~shows cloud inhomogeneities in CDNCon different scales (Fig.8).~~ $_h^a$ reveals areas of increased and decreased CDNC. For example, profile 7 shows regions of ~~lower~~ decreased CDNC, whereas profile 9 shows regions of ~~higher~~ increased CDNC compared to the mean profile. The CDNC at 1100 m in profile 9 (200 cm^{-3}) is more than a factor 3 higher than in profile 7 (60 cm^{-3}). ~~Assuming a mean wind speed of 10 m s^{-1}, these translates to an inter-profile variability in CDNC on a scale of 30 km. From an intra-profile variability perspective, on a scale of tens of meters,~~ From a single profile perspective, all profiles show alternating regions of higher and lower CDNC. ~~For example, CDNC in profile 7 increases by a factor of 1.7 in the 10 m height interval between 1100 m (58 cm^{-3}) and 1120 m (100 cm^{-3}).~~ It is likely that the observed variations in CDNC exceed statistical variations and are the result of different ~~cloud processes. Upon further analysis, we investigate various physical processes, which could explain these cloud inhomogeneities on different scales~~physical processes.

The variability in CDNC on a scale of several kilometers might be explained by ~~internal gravity waves in the boundary layer.~~ the presence of boundary layer waves. Boundary layer waves can cause entrainment of dry air into the cloud (Mellado, 2017) and could affect the cloud structure (e.g. Bergot, 2013). As discussed for example by Wanner and Furger (1990), strengthening or weakening of the Bise due to dynamic ~~or orographic~~ effects could induce oscillations within the cold air and lead to the formation of boundary layer waves at the cloud top. The ~~questions is whether these boundary layer waves can propagate~~

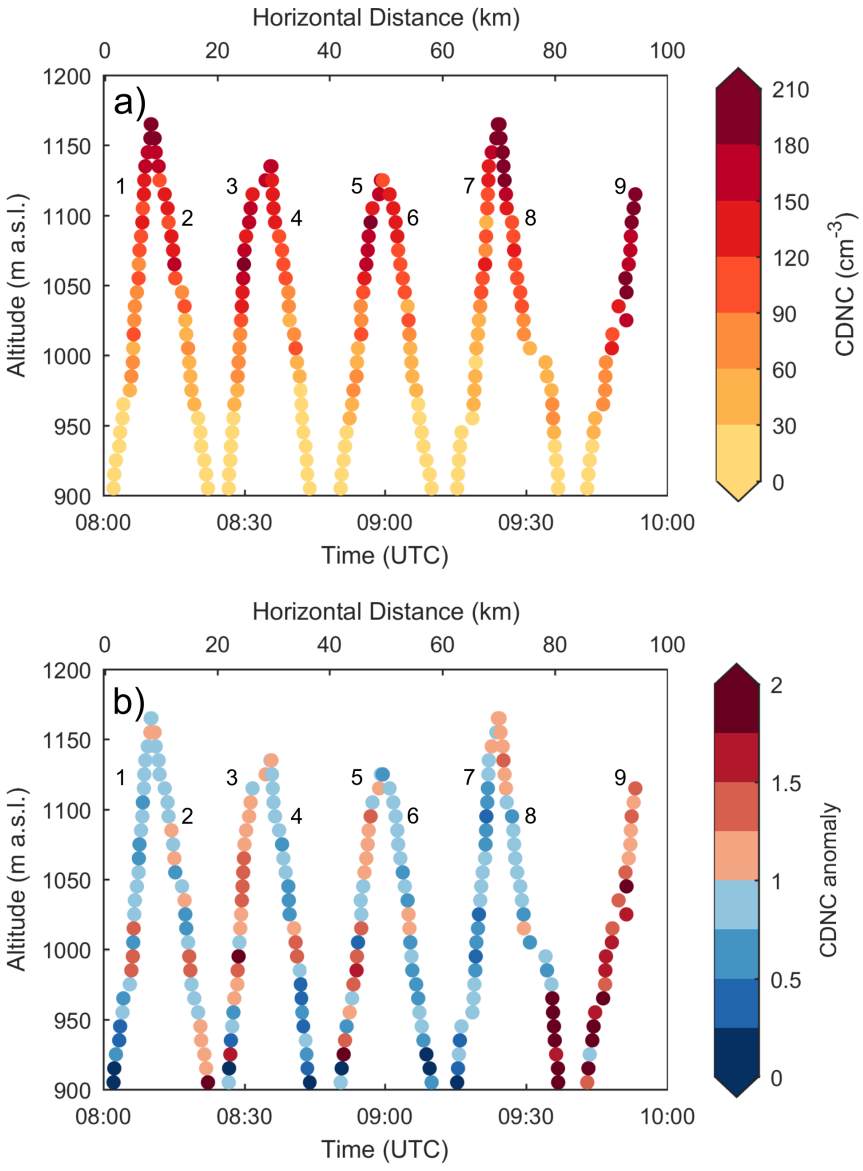

Figure 8. Height-temporal evolution of the CDNC (top) and the CDNC anomaly (CDNC$_h^a$, bottom) (see text for explanation of anomaly). The data points are averaged over an altitude interval of 10 m. The upper x-axis shows the horizontal distance s of the cloud, assuming a mean wind speed v of 10 m s^{-1} over time t ($s = v \cdot t$). The numbers represent the profile number according to Table 2.

~~through the cloud and explain the variability in CDNC. The~~ presence of wind shear and a positive Brunt-Väisälä frequency (N= 0.04 s^{-1}) at the inversion (see Fig. 6.e) ~~suggests that Kelvin-Helmholtz instability occurs at the cloud top, which is a favourable condition~~ represent favourable conditions for the formation of Kelvin-Helmholtz instability and boundary layer waves. ~~These~~

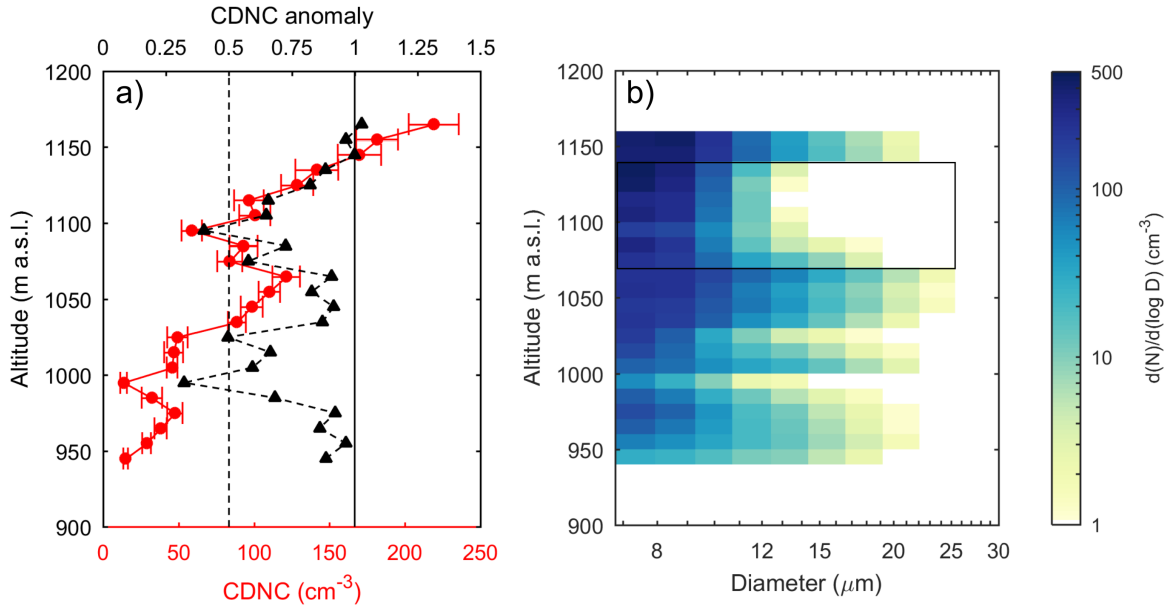

Figure 9. Vertical profile of CDNC (in red) and CDNC anomaly (in black, $CDNC_h^a$) (left) and number size distribution (right) of profile 7. ~~The CDNC is shown by~~ To the ~~red solid line and~~ left of the ~~CDNC anomaly by the black~~ dashed ~~line (see text for explanation of anomaly). The black dashed~~ vertical line ~~indicates regions of decreased~~ in Fig. 9.a, CDNC~~($CDNC_h^a$ <~~is less than 0.5~~)~~. The data is averaged over a 10 m interval. The ~~dashed rectangles~~ black rectangle in Fig.9.b shows the ~~number size distribution plot show regions~~ region of decreased CDNC (discussed in text).

~~boundary layer waves can penetrate dry air into the cloud and could affect the cloud microphysics (e.g. Bergot 2013). The penetration depth depends on different factors such as the relative humidity above the cloud, the temperature stratification of the atmosphere, the turbulence conditions and the cloud water content (Korolev and Mazin, 1993). Kelvin-Helmholtz instability can enhance mixing and modify entrainment at the cloud top (Mellado, 2017) and thus influence the cloud microstructure. However,~~ However, in order to further test this hypothesis, microphysical observations up to cloud top and an extended set of ~~wind measurements~~ auxiliary measurements (e.g. three-dimensional wind field, turbulence) over a time period of several hours would be necessary~~to further test the hypothesis of boundary layer waves influencing the structure of clouds~~.

~~Cloud inhomogeneities~~ Inhomogeneities in CDNC on a meter scale can be the result of different processes, depending on their location within the cloud. We will discuss these cloud inhomogeneities based on ~~the~~ profile 7, because it ~~shows regions of decreased CDNC~~has $CDNC_h^a$ below 1 almost everywhere (see Fig. 8.b). ~~The cloud droplet number size distribution of profile~~ Profile 7 shows a gradual increase in cloud droplet size and number concentration with height until a sudden decrease in particle concentration and cloud droplet size occurs between 1070 m and 1130 m (Fig. 9.b). In this region, CDNC is less than half of the average CDNC ($CDNC_h^a < 0.5$, Fig. 9.a). In addition, the cloud droplet spectrum shows an increase of ~~CDNC of~~ small droplets and an absence of cloud droplets larger than 14 µm. Korolev and Mazin (1993) propose several mechanisms for the formation of

cloud inhomogeneities on a meter scale such as (i) entrainment, (ii) variability of the condensation level and (iii) evaporation in descending motions. Considering the location of our region of decreased CDNC (300-400 m from cloud top, 200 m from cloud base), we assume that this CDNC$_b^a$ below 1 is most likely formed by evaporation in descending motions. The temperature inside a descending air parcel increases due to adiabatic compression and heating and in response cloud droplets evaporate leading to regions of decreased CDNC. ~~According to the calculations in Korolev and Mazin (1993), a vertical displacement ΔZ^* of 60 m would be necessary for complete droplet evaporation of a cloud parcel with an initial LWC of 0.1 g kg^{-1}, assuming no mixing and an adiabatic gradient of specific LWC β_{ad} of $1.6 \cdot 10^{-3}$ g kg^{-1} (T =273 K and p = 900 mb). As we observed similar initial conditions, these calculations support the hypothesis that the region of decreased CDNC between 1070 m and 1130 m was formed by droplet evaporation in a descending air parcel. Even though radiative cooling or the Kelvin-Helmholtz instability could enhance entrainment at the cloud top, it is unlikely that entrainment influences the cloud structure 300-400 m below the cloud base.Similarly, a sudden decrease in the CDNC is observed at around 1000 m. Unlike the decrease between 1070 m and 1130 m, a decrease of both the small and large droplets is observed, suggesting that another mechanism is occurring. Based on the location within the cloud and the decrease of small and large droplets, we assume that this region of decreased CDNC could be explained by irregularities of the condensation level (e.g. Korolev and Mazin 1993). These irregularities could be due to fluctuations in temperature or humidity close to the cloud base. This could lead to homogeneous mixing of the cloudy and cloud-free volumes and thus to a decrease of both CDNC and size.~~

5 ~~Discussion~~

4.1 ~~Clouds - a complex multi-scale phenomenon~~

~~Overview image summarizing the observed cloud inhomogeneities on different scale (top) and discussing multiple cloud processes, which could explain these cloud inhomogeneities (bottom).Even though high fog and stratus clouds are of stratiform nature, we found that stratus clouds are complex dynamic structures with cloud inhomogeneities on different scales. The results of the case study are summarized and conceptualized in Fig. 10. These cloud inhomogeneities represent and influence various processes on a wide range of scales.Inhomogeneities on scales of several kilometers can play an important role for cloud radiative effects (Slingo, 1990). These inhomogeneities can be formed for example by internal gravity waves in the boundary layer due to topographic effects or dynamical instabilities. We found conditions favorable for the formation of boundary layer waves and Kelvin-Helmholtz instabilities at the cloud top (e.g. wind shear, stable stratification). The Brunt-Väisälä frequency indicates a wave period of around 2-3 minutes, which is at the lower range of typical boundary layer waves. These boundary layer waves could propagate into the cloud (Fig. 10, bottom left), influence the cloud microphysical processes and explain the observed variabilities in CDNC on a scale of tens of kilometers (Fig. 10, top left). Previous studies suggested that boundary layer waves and Kelvin-Helmholtz instabilities near the cloud top could affect the cloud microphysics. For example, a large-eddy simulation study by Bergot (2013) showed that eddies near the cloud top influenced the fog microphysics of the fog layer and that the observed fluctuations in LWC close to the cloud top can have a strong impact on the radiative fluxes.Cloud inhomogeneities on a meter scale can be the result of different processes. For example, we observed a sudden~~

decrease in CDNC and cloud droplet size in a 50 m height interval within the cloud. We assume that this is the result of adiabatic compression and heating and subsequent droplet evaporation in a downdraft region of an eddy (Fig. 10, bottom center). Furthermore, we observed a region of decreased CDNC and size close to the cloud base. We hypothesize that this region of decreased CDNC is formed by irregularities in the condensation level. Previous studies have found cloud inhomogeneities in cloud properties on a meter scale (e.g. Korolev and Mazin 1993, Gerber et al. 2005). For example, Gerber et al. (2005) found regions with sharply reduced LWC compared to the background in stratocumulus clouds ('cloud holes'), which were assumed to be the result of entrainment of dry air. Similarly, García-García et al. (2002) observed regions of decreased CDNC of a few tens of meters in warm fog characterized by a broader droplet size distribution. These inhomogeneities on a meter scale can influence the cloud droplet size distribution and thus play an important role in the evolution of the cloud.Inhomogeneities on the centimeter and millimeter scale can influence precipitation initiation and the radiative properties of clouds. Several studies (e.g. Baker 1992, Brenguier 1993, Beals et al. 2015) observed sharp transitions at the interface between cloud and ambient air on the centimeter scale as a response to entrainment and mixing. Moreover, these inhomogeneities on the microscale can influence growth by collision-coalescence or the Wegener-Bergeron-Findeisen process and thus the efficiency of precipitation formation. The ability of HOLIMO to detect the spatial distribution of particles in a cloud volume allows studying these small-scale processesHowever, more sophisticated analyses of turbulence and microphysical observations up to cloud top are required to further investigate these cloud inhomogeneities and particle-particle interactions on a millimeter scale (Fig. 10, top right). However, a quantitative analysis of the spatial distribution (e.g. Larsen and Shaw (2018), Larsen et al. (2018)) is required to assess these small-scale processes, the corresponding physical processes, which is beyond the scope of this study. The results presented here and previous studies show that cloud inhomogeneities on different scales occur in clouds. It is still not fully understood how these cloud inhomogeneities are formed, how these inhomogeneities influence the evolution of the cloud structure and how they interact on different scales. With HoloBalloon, we bring together a wide range of scales from the kilometer down to the millimeter scale. Such a multi-scale approach could help to improve the understanding the inhomogeneous, dynamic and complex nature of clouds.

5 Discussion

5.1 Deploying a TBS in Validation of the fieldHoloBalloon platform and further improvements

The HoloBalloon platform was successfully deployed in various meteorological conditions. In situ profiles up to 700 m altitude above the ground were obtained, limited by air traffic restrictions in the maximum altitude. Unfortunately, because of this limitation in the maximum altitude, we were not able to penetrate the whole cloud layer and perform measurements at the cloud top. The platform was deployed at temperatures down to -8 °C. Despite the supercooled conditions, we observed only a few ice crystals (<1 0.1 L^{-1}). Even though parts of the balloon and of the cable were covered in ice, this did not affect our measurements and the flight performance. However, based on our experience, we recommend covering the balloon with a tarpaulin tarp during night to prevent accumulation of snow and water on the balloon. We flew the TBS in wind speeds up to 15 m s^{-1}. The TBS was stable in these high wind conditions, but the ground handling became challenging at wind speeds

above 10 m s^{-1}, especially in the presence of wind gusts.

~~Regarding the effort for~~ For setting up and operating the HoloBalloon platform, several aspects ~~should~~ need to be considered. Firstly, a closed air space was required to perform cloud measurements with a TBS. The process of obtaining a closed air space was closely coordinated with the aviation safety authority. In areas with dense air traffic, such as the Swiss Plateau, it can be difficult to find a suitable location. Secondly, a large, reasonably flat surface area (~20 m×40 m) is required to prepare and launch the TBS. No major obstacles (e.g. trees, power lines) should be within a radius of around 60 m of the launching site and it should be possible to insert an anchor into the ground. The system set up takes approximately 3 days and requires 2-3 trained persons for operation. A third person can especially be helpful during difficult wind conditions.

HoloBalloon was able to measure temperature, relative humidity and wind profiles in boundary layer clouds. In general, the measurements agreed well with the observations from the MeteoSwiss weather stations and the radiosondes (see Fig. 6). The temperature sensor showed a delayed response to changes in the ambient temperature (not shown), ~~as was observed~~ similarly to what was observed by Beck et al. (2017) on the cable car platform HoloGondel~~(Beck et al., 2017)~~. To overcome this issue, the temperature was calculated from the virtual temperature of the 3D sonic anemometer, assuming water saturation in the cloud. It is well known that it is difficult to measure relative humidity in clouds (e.g. ~~Korolev and Mazin 2003, Korolev and Isaac 2006~~ Korolev and Mazin, 2003; Korolev and Isaac, 2006). The relative humidity measured by the HoloBalloon platform in clouds ranged between 93 % and 98 %. We assumed in-cloud conditions when the relative humidity remained constant with height. Wind speed and direction measurements of the 3D sonic anemometer were corrected for the motion of the balloon. As described in Sect. 2, this was done using the output from an inertial navigation system and a GPS antenna following the procedure described in ~~Mellado (2017)~~Elston et al. (2015). The corrected horizontal wind speed and wind direction measurements agreed well with the radiosonde observations. ~~The vertical wind speed was~~ Vertical wind speed and turbulence measurements were not considered in this study~~. Although turbulence was not the focus of this study, turbulence measurements should be interpreted with caution. As~~ , because we cannot exclude an influence from the balloon on the turbulence measurements, as the instrument package was installed on the ~~kiel~~ keel below the balloon (Fig.~~1), we cannot exclude an influence from the balloon~~ 1). For future field campaigns, ~~the feasibility of installing the instrument package 30-40~~we will install the instrument package 20-30 m below the balloon ~~should be assessed.~~ in order to minimize potential influences from the balloon and to analyze also turbulence data of the 3D sonic anemometer. The feasibility of a hanging mount was already successfully tested in the field in the fall of 2019. The vertical profiles of the microphysical measurement showed no systematic difference between ascending and descending profiles (see Fig. 8.b), suggesting that the balloon was not significantly influencing the microphysical measurements themselves. With a mean horizontal wind speed of 10 m s^{-1} and a cable speed of 1 m s^{-1}, the horizontal wind speed is by a factor 10 larger than the cable speed. This, in combination with a flight angle of up to 45° (due to the kytoon design), ~~prevents~~ minimizes shading effects and further support the assumption that a 'pristine' cloud volume is measured.

Generally, the measured size distributions during the present case study showed the maximum number concentration close to the resolution limit of HOLIMO 3B. This demonstrates the limits of the instrument in measuring small cloud particles (< 6 µm). This bias can lead to an underestimation of CDNC, especially close to cloud base or in fog or clouds with a small mean cloud droplet diameter. For future field campaigns, ~~instruments measuring cloud particles below 6 m would be helpful~~

~~(e.g. optical particle counter), especially in fog or clouds with small mean cloud diameters in order to cover the entire cloud droplet spectrum.~~ we will equip the HoloBalloon platform with an optical particle counter in order to cover the entire cloud droplet size distribution.

~~HoloBalloon has proven its ability to measure in situ vertical profiles of microphysical and meteorological cloud properties~~

5.2 Using the HoloBalloon platform to study boundary layer clouds

The potential of the HoloBalloon platform in studying boundary layer clouds is summarized in a conceptual picture (Fig. 10), which is described with the help of the presented case study. Based on the research questions, different analysis strategies can be applied. Firstly, by analyzing a series of vertical profiles, the HoloBalloon platform can investigate the temporal and spatial evolution of cloud properties on a kilometer scale (Fig. 10, top). A vertical profile of 500 m can be accomplished within 8 minutes. Thus, a vertical profile can be obtained faster than with an aircraft. Secondly, individual profiles obtained with the HoloBalloon platform can provide information about the vertical cloud structure (Fig. 10, middle). With a sample rate of up to 80 fps and an aspiration speed on the order of 10 m s^{-1}, the HoloBalloon platform can provide high-resolution measurements on the meter scale. We found that stratus clouds can exhibit complex dynamic structures with microphysical signatures on different scales (Sect. 4.4). For example, we observed a large variability in the CDNC and cloud droplet size within the stratus cloud. More sophisticated analyses of numerous cloud cases are required to further investigate cloud inhomogeneities and their physical implications. However, no generalization was possible in this study.

Furthermore, the analysis of individual holograms, or more specifically the analysis of the spatial distribution of an ensemble of cloud particles in the sample volume (Fig. 10, bottom), allows studying small-scale processes and particle-particle interactions. For example, a spatial distribution analysis can provide insights of the physical nature of the interface between cloudy and ambient air and thus can be used to study entrainment and turbulent mixing at the cloud top. However, a quantitative analysis of the spatial distribution (e.g. Larsen and Shaw, 2018; Larsen et al., 2018) is required to assess these small-scale processes, which is beyond the scope of this study. Future work will focus on the spatial distribution of cloud particles.

The HoloBalloon platform can be used to study processes over a wide range of scales from the kilometer down to the millimeter scale. However, the present case study also revealed some limitations of the HoloBalloon platform. For example, the vertical profiles are limited by the cable length (1200 m) or air traffic regulations regarding the maximum flight height (700 m) and it can only observe the cloud properties along the measurement path. In order to obtain a more comprehensive understanding of boundary layer clouds~~up to 700 meters above ground.~~, a multi-dimensional set of instruments would be necessary. For example, the HoloBalloon measurements could be complemented by remote sensing instruments (e.g. cloud radar), which can provide continuous information of the large-scale cloud structure. Moreover, a wind profiler could be used to characterize the three-dimensional wind field and to identify dynamical patterns such as boundary layer waves. Such a multi-scale approach could help to improve the microphysical and dynamical understanding of boundary layer clouds in future field campaigns.

6 Conclusions

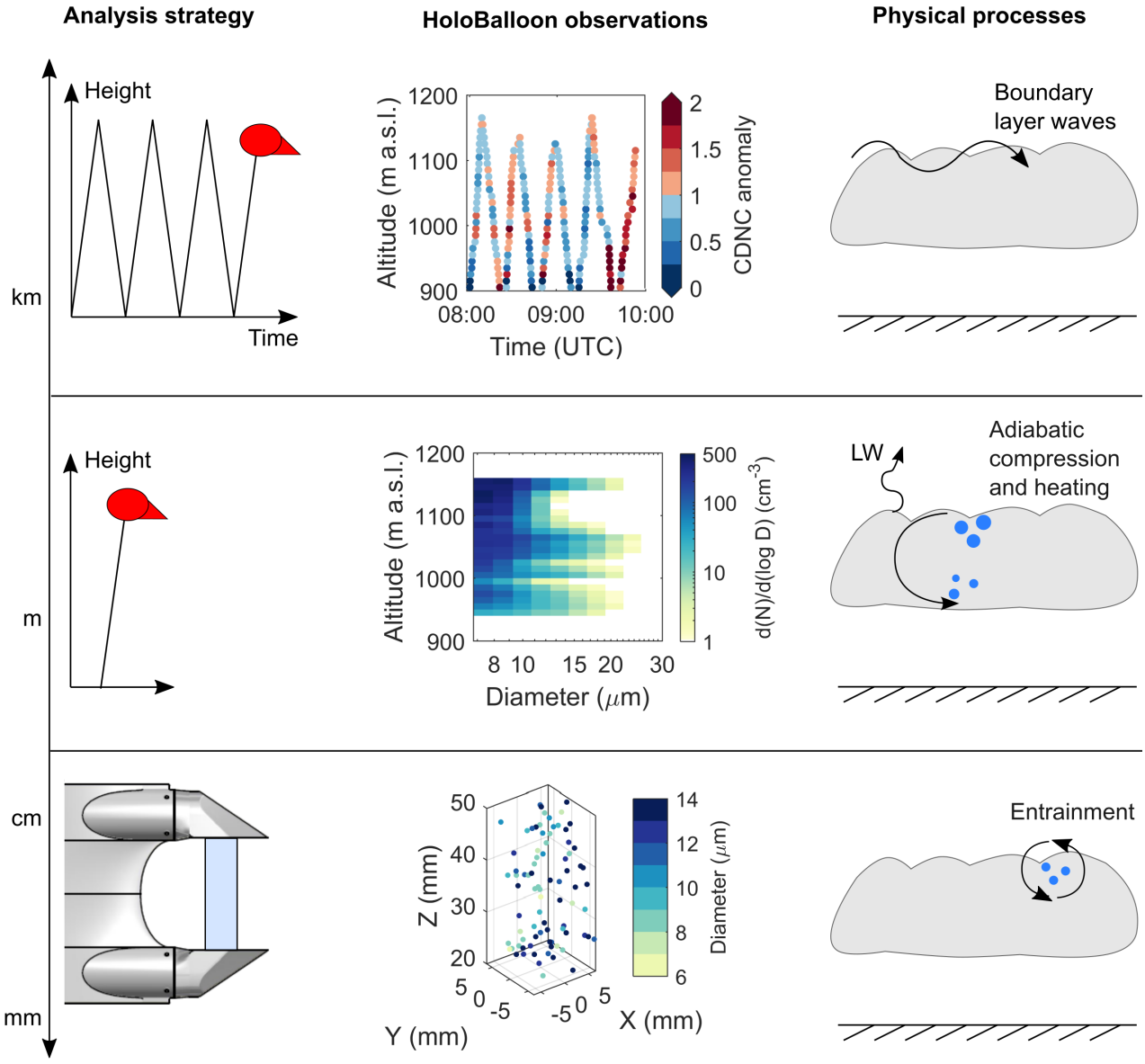

Figure 10. Conceptual picture describing the potential of the HoloBalloon platform in studying boundary layer clouds. It shows the scale-dependent analysis strategy (left), exemplary HoloBalloon observations of the presented case study (center) and possible physical processes that can be studied with the HoloBalloon platform (right). The scale-dependent analysis strategies include the analysis of a series of vertical profiles (top), a single vertical profile (middle) and a single hologram (bottom).

In this study, we have introduced the newly developed measurement platform HoloBalloon and have shown its ability and potential in studying boundary layer clouds. Here, we presented in situ observations of a supercooled low stratus cloud during a Bise event over the Swiss Plateau in February 2018. Our main findings are summarized as follows:

- HoloBalloon merges the advantages of holography with the benefits of a TBS. Unlike other single cloud particle instrumentation, holographic cloud imagers have a well-defined sample volume independent of particle size and air speed despite fluctuating aspiration speeds on a TBS. The low aspiration speed on the TBS in combination with the high acquisition rate of HOLIMO 3B allows for measurements with high spatial resolution.

- The HoloBalloon platform was successfully deployed at temperatures down to -8 °C and wind speeds up to 15 $\mathrm{m\,s^{-1}}$. While conventional blimp-like TBS are limited to wind speeds below 10 $\mathrm{m\,s^{-1}}$, kytoons are designed for wind speeds up to 25 $\mathrm{m\,s^{-1}}$, making them an interesting measurement platform for atmospheric research.

- HoloBalloon was able to reliable measure in situ vertical profiles of the microphysical cloud properties and meteorological parameters up to 700 meters above ground. The meteorological measurements agreed well with observations from radiosondes and weather stations and the observed cloud properties were within the expected range for fog and stratus clouds. Cloud particles between 6 µm and 24 µm and CDNC up to 200 $\mathrm{cm^{-3}}$ were observed with HOLIMO 3B.

- HoloBalloon was able to capture cloud inhomogeneities on different scales. For example, we observed ~~variability of CDNC~~ a large variability in the CDNC and mean cloud droplet diameter from a kilometer down to a meter scale. ~~Boundary layer waves or Kelvin-Helmholtz instability at the cloud top connected to the Bise situation influenced the cloud structure on a kilometer scale. Moreover, we observed cloud regions with decreased CDNC and cloud droplet size on a scale of 30-50 m, likely caused by droplet~~ We hypothesize that boundary layer waves and droplet evaporation in a descending air parcel ~~. In addition, HOLIMO~~ might have influenced the cloud structure. However, further analyses are required to investigate these hypotheses. Moreover, HOLIMO 3B is capable of measuring the spatial distribution of ~~cloud particles in a cloud volume~~ an ensemble of cloud particles on a millimeter scale (e.g. ~~Beals et al. 2015, Beck et al. 2017~~ Beals et al., 2015; Beck et al., 2017). This outstanding feature of holography allows studying processes on the particle scale such as ~~mixing of cloudy and dry air or growth by collision-coalescence, which can be important for precipitation formation. Lastly, the modular design of the HoloBalloon platform allows for varying research questions to be addressed. For example,~~ entrainment, turbulent mixing or cloud particle growth.

- For future balloon-borne cloud measurements we recommend to install the instrument package ~~can be modified to include aerosol, radiation or turbulence measurements. Additionally, the measurement platform could be installed 30-50~~20 - 30 m below the balloon to ~~avoid any interference~~ reduce potential influences from the balloon ~~itself. Furthermore, future field campaigns will include an optical particle counter to extend the~~ on the cloud and turbulence measurements. In addition, we recommend that instruments covering the entire cloud particle spectrum ~~to particles below 6 m.~~ are installed to accurately capture cloud activation and entrainment.

Code and data availability.

Author contributions. FR prepared the manuscript with contributions from AB, JH and UL. FR and JH performed the HoloBalloon measurements. FR analyzed the HoloBalloon measurements and FR, AB, JH and UL interpreted the data.

Competing interests. The authors declare that they have no conflict of interest.

Acknowledgements. The authors would like to thank Jörg Wieder for his assistance during the size calibration experiments and Julie Pasquier for the analysis of the resolution measurement. We also thank Hannes Wydler and Michael Rösch for their technical support in designing the HoloBalloon platform. The authors also thank the Kieswerk Risi and the Gemeinde Aarwangen for their excellent support during the field campaign. We would also like to thank the Federal Office of Civil Aviation (FOCA) for their assistance in getting the flight permit. The meteorological measurements were provided by the Swiss Federal Office of Meteorology and Climatology MeteoSwiss. This project was supported by the ETH Scientific Equipment Program.

References

Amsler, P., Stetzer, O., Schnaiter, M., Hesse, E., Benz, S., Moehler, O., and Lohmann, U.: Ice crystal habits from cloud chamber studies obtained by in-line holographic microscopy related to depolarization measurements, Applied optics, 48, 5811–5822, 2009.

Baker, B. A.: Turbulent entrainment and mixing in clouds: A new observational approach, Journal of the atmospheric sciences, 49, 387–404, 1992.

Bartok, J., Bott, A., and Gera, M.: Fog prediction for road traffic safety in a coastal desert region, Boundary-layer meteorology, 145, 485–506, 2012.

Baumgardner, D., Brenguier, J., Bucholtz, A., Coe, H., DeMott, P., Garrett, T., Gayet, J., Hermann, M., Heymsfield, A., Korolev, A., et al.: Airborne instruments to measure atmospheric aerosol particles, clouds and radiation: A cook's tour of mature and emerging technology, Atmospheric Research, 102, 10–29, 2011.

Beals, M. J., Fugal, J. P., Shaw, R. A., Lu, J., Spuler, S. M., and Stith, J. L.: Holographic measurements of inhomogeneous cloud mixing at the centimeter scale, Science, 350, 87–90, 2015.

Beck, A.: Observing the Microstructure of Orographic Clouds with HoloGondel, Ph.D. thesis, ETH Zurich, 2017.

Beck, A., Henneberger, J., Schöpfer, S., Fugal, J., and Lohmann, U.: HoloGondel: in situ cloud observations on a cable car in the Swiss Alps using a holographic imager, Atmospheric Measurement Techniques, 10, 459–476, 2017.

Beck, A., Henneberger, J., Fugal, J. P., David, R. O., Lacher, L., Lohmann, U., and Möhler, O.: Impact of surface and near-surface processes on ice crystal concentrations measured at mountain-top research stations., Atmospheric Chemistry & Physics, 18, 2018.

Bendix, J.: A satellite-based climatology of fog and low-level stratus in Germany and adjacent areas, Atmospheric Research, 64, 3–18, 2002.

Bennartz, R.: Global assessment of marine boundary layer cloud droplet number concentration from satellite, Journal of Geophysical Research: Atmospheres, 112, 2007.

Bergot, T.: Small-scale structure of radiation fog: a large-eddy simulation study, Quarterly Journal of the Royal Meteorological Society, 139, 1099–1112, 2013.

Bergot, T., Terradellas, E., Cuxart, J., Mira, A., Liechti, O., Mueller, M., and Nielsen, N. W.: Intercomparison of single-column numerical models for the prediction of radiation fog, Journal of applied meteorology and climatology, 46, 504–521, 2007.

Borrmann, S., Jaenicke, R., and Neumann, P.: On spatial distributions and inter-droplet distances measured in stratus clouds with in-line holography, Atmospheric research, 29, 229–245, 1993.

Brenguier, J.-L.: Observations of cloud microstructure at the centimeter scale, Journal of Applied Meteorology, 32, 783–793, 1993.

Canut, G., Couvreux, F., Lothon, M., Legain, D., Piguet, B., Lampert, A., Maurel, W., and Moulin, E.: Turbulence fluxes and variances measured with a sonic anemometer mounted on a tethered balloon, Atmospheric Measurement Techniques, 9, 4375–4386, 2016.

Cermak, J. and Bendix, J.: A novel approach to fog/low stratus detection using Meteosat 8 data, Atmospheric Research, 87, 279–292, 2008.

Cermak, J., Eastman, R. M., Bendix, J., and Warren, S. G.: European climatology of fog and low stratus based on geostationary satellite observations, Quarterly Journal of the Royal Meteorological Society: A journal of the atmospheric sciences, applied meteorology and physical oceanography, 135, 2125–2130, 2009.

Conway, B., Caughey, S., Bentley, A., and Turton, J.: Ground-based and airborne holography of ice and water clouds, Atmospheric Environment (1967), 16, 1193–1207, 1982.

Creamean, J. M., Primm, K. M., Tolbert, M. A., Hall, E. G., Wendell, J., Jordan, A., Sheridan, P. J., Smith, J., and Schnell, R. C.: HOVERCAT: a novel aerial system for evaluation of aerosol-cloud interactions., Atmospheric Measurement Techniques, 11, 2018.

Desai, N., Glienke, S., Fugal, J., and Shaw, R.: Search for microphysical signatures of stochastic condensation in marine boundary layer clouds using airborne digital holography, Journal of Geophysical Research: Atmospheres, 124, 2739–2752, 2019.

Elston, J., Argrow, B., Stachura, M., Weibel, D., Lawrence, D., and Pope, D.: Overview of small fixed-wing unmanned aircraft for meteorological sampling, Journal of Atmospheric and Oceanic Technology, 32, 97–115, 2015.

Fabbian, D., de Dear, R., and Lellyett, S.: Application of artificial neural network forecasts to predict fog at Canberra International Airport, Weather and forecasting, 22, 372–381, 2007.

Fugal, J. P. and Shaw, R. A.: Cloud particle size distributions measured with an airborne digital in-line holographic instrument, Atmospheric Measurement Techniques, 2, 259–271, 2009.

Fugal, J. P., Schulz, T. J., and Shaw, R. A.: Practical methods for automated reconstruction and characterization of particles in digital in-line holograms, Measurement Science and Technology, 20, 075 501, 2009.

Garcıa-Garcıa, F., Virafuentes, U., and Montero-Martınez, G.: Fine-scale measurements of fog-droplet concentrations: A preliminary assessment, Atmospheric research, 64, 179–189, 2002.

Gerber, H., Frick, G., Malinowski, S., Brenguier, J., and Burnet, F.: Holes and entrainment in stratocumulus, Journal of the atmospheric sciences, 62, 443–459, 2005.

Glienke, S., Kostinski, A., Fugal, J., Shaw, R., Borrmann, S., and Stith, J.: Cloud droplets to drizzle: Contribution of transition drops to microphysical and optical properties of marine stratocumulus clouds, Geophysical Research Letters, 44, 8002–8010, 2017.

Gultepe, I., Tardif, R., Michaelides, S., Cermak, J., Bott, A., Bendix, J., Müller, M. D., Pagowski, M., Hansen, B., Ellrod, G., et al.: Fog research: A review of past achievements and future perspectives, Pure and Applied Geophysics, 164, 1121–1159, 2007.

Hartmann, D. L., Ockert-Bell, M. E., and Michelsen, M. L.: The effect of cloud type on Earth's energy balance: Global analysis, Journal of Climate, 5, 1281–1304, 1992.

Henneberger, J., Fugal, J., Stetzer, O., and Lohmann, U.: HOLIMO II: a digital holographic instrument for ground-based in situ observations of microphysical properties of mixed-phase clouds, Atmospheric Measurement Techniques, 6, 2975–2987, 2013.

Köhler, C., Steiner, A., Saint-Drenan, Y.-M., Ernst, D., Bergmann-Dick, A., Zirkelbach, M., Bouallègue, Z. B., Metzinger, I., and Ritter, B.: Critical weather situations for renewable energies–Part B: Low stratus risk for solar power, Renewable Energy, 101, 794–803, 2017.

Korolev, A. and Isaac, G. A.: Relative humidity in liquid, mixed-phase, and ice clouds, Journal of the atmospheric sciences, 63, 2865–2880, 2006.

Korolev, A. and Mazin, I.: Zones of increased and decreased droplet concentration in stratiform clouds, Journal of Applied Meteorology, 32, 760–773, 1993.

Korolev, A., Emery, E., Strapp, J., Cober, S., Isaac, G., Wasey, M., and Marcotte, D.: Small ice particles in tropospheric clouds: Fact or artifact? Airborne Icing Instrumentation Evaluation Experiment, Bulletin of the American Meteorological Society, 92, 967–973, 2011.

Korolev, A. V. and Mazin, I. P.: Supersaturation of water vapor in clouds, Journal of the atmospheric sciences, 60, 2957–2974, 2003.

Kozikowska, A., Haman, K., and Supronowicz, J.: Preliminary results of an investigation of the spatial distribution of fog droplets by a holographic method, Quarterly Journal of the Royal Meteorological Society, 110, 65–73, 1984.

Larsen, M. L. and Shaw, R. A.: A method for computing the three-dimensional radial distribution function of cloud particles from holographic images, Atmospheric Measurement Techniques, 11, 4261–4272, 2018.

Larsen, M. L., Shaw, R. A., Kostinski, A. B., and Glienke, S.: Fine-scale droplet clustering in atmospheric clouds: 3D radial distribution function from airborne digital holography, Physical review letters, 121, 204 501, 2018.

Lawson, R. P., Stamnes, K., Stamnes, J., Zmarzly, P., Koskuliks, J., Roden, C., Mo, Q., Carrithers, M., and Bland, G. L.: Deployment of a tethered-balloon system for microphysics and radiative measurements in mixed-phase clouds at Ny-Ålesund and South Pole, Journal of Atmospheric and Oceanic Technology, 28, 656–670, 2011.

Liu, Y., Shupe, M. D., Wang, Z., and Mace, G.: Cloud vertical distribution from combined surface and space radar-lidar observations at two Arctic atmospheric observatories, Atmospheric Chemistry and Physics (Online), 17, 2017.

Lloyd, G., Choularton, T., Bower, K., Gallagher, M., Connolly, P., Flynn, M., Farrington, R., Crosier, J., Schlenczek, O., Fugal, J., et al.: The origins of ice crystals measured in mixed-phase clouds at the high-alpine site Jungfraujoch, Atmospheric Chemistry and Physics, 15, 12 953–12 969, 2015.

Lohmann, U., Lüönd, F., and Mahrt, F.: An introduction to clouds: From the microscale to climate, Cambridge University Press, 2016.

Maletto, A., McKendry, I., and Strawbridge, K.: Profiles of particulate matter size distributions using a balloon-borne lightweight aerosol spectrometer in the planetary boundary layer, Atmospheric Environment, 37, 661–670, 2003.

Marchand, R., Mace, G. G., Ackerman, T., and Stephens, G.: Hydrometeor detection using CloudSat—An Earth-orbiting 94-GHz cloud radar, Journal of Atmospheric and Oceanic Technology, 25, 519–533, 2008.

Mazzola, M., Busetto, M., Ferrero, L., Viola, A. P., and Cappelletti, D.: AGAP: an atmospheric gondola for aerosol profiling, Rendiconti Lincei, 27, 105–113, 2016.

Mellado, J. P.: Cloud-top entrainment in stratocumulus clouds, Annual Review of Fluid Mechanics, 49, 145–169, 2017.

Miles, N. L., Verlinde, J., and Clothiaux, E. E.: Cloud droplet size distributions in low-level stratiform clouds, Journal of the atmospheric sciences, 57, 295–311, 2000.

Müller, M. D., Masbou, M., and Bott, A.: Three-dimensional fog forecasting in complex terrain, Quarterly Journal of the Royal Meteorological Society, 136, 2189–2202, 2010.

Pagowski, M., Gultepe, I., and King, P.: Analysis and modeling of an extremely dense fog event in southern Ontario, Journal of applied meteorology, 43, 3–16, 2004.

Randall, D., Coakley Jr, J., Fairall, C., Kropfli, R., and Lenschow, D.: Outlook for research on subtropical marine stratiform clouds, Bulletin of the American Meteorological Society, 65, 1290–1301, 1984.

Raupach, S., Vössing, H., Curtius, J., and Borrmann, S.: Digital crossed-beam holography for in situ imaging of atmospheric ice particles, Journal of Optics A: Pure and Applied Optics, 8, 796, 2006.

Rees, J., Denholm-Price, J., King, J., and Anderson, P.: A climatological study of internal gravity waves in the atmospheric boundary layer overlying the Brunt Ice Shelf, Antarctica, Journal of the atmospheric sciences, 57, 511–526, 2000.

Román-Cascón, C., Steeneveld, G., Yagüe, C., Sastre, M., Arrillaga, J., and Maqueda, G.: Forecasting radiation fog at climatologically contrasting sites: evaluation of statistical methods and WRF, Quarterly Journal of the Royal Meteorological Society, 142, 1048–1063, 2016.

Sassen, K., Mace, G. G., Wang, Z., Poellot, M. R., Sekelsky, S. M., and McIntosh, R. E.: Continental stratus clouds: A case study using coordinated remote sensing and aircraft measurements, Journal of the atmospheric sciences, 56, 2345–2358, 1999.

Schlenczek, O.: Airborne and Ground-based Holographic Measurement of Hydrometeors in Liquid-phase, Mixed-phase and Ice Clouds, Ph.D. thesis, Universitätsbibliothek Mainz, 2018.

Schlenczek, O., Fugal, J. P., Lloyd, G., Bower, K. N., Choularton, T. W., Flynn, M., Crosier, J., and Borrmann, S.: Microphysical properties of ice crystal precipitation and surface-generated ice crystals in a High Alpine environment in Switzerland, Journal of Applied Meteorology and Climatology, 56, 433–453, 2017.

Siebert, H., Wendisch, M., Conrath, T., Teichmann, U., and Heintzenberg, J.: A new tethered balloon-borne payload for fine-scale observations in the cloudy boundary layer, Boundary-layer meteorology, 106, 461–482, 2003.

Siebert, H., Franke, H., Lehmann, K., Maser, R., Saw, E. W., Schell, D., Shaw, R. A., and Wendisch, M.: Probing finescale dynamics and microphysics of clouds with helicopter-borne measurements, Bulletin of the American Meteorological Society, 87, 1727–1738, 2006.

Sikand, M., Koskulics, J., Stamnes, K., Hamre, B., Stamnes, J., and Lawson, R.: Estimation of mixed-phase cloud optical depth and position using in situ radiation and cloud microphysical measurements obtained from a tethered-balloon platform, Journal of the Atmospheric Sciences, 70, 317–329, 2013.

Slingo, A.: Sensitivity of the Earth's radiation budget to changes in low clouds, Nature, 343, 49, 1990.

Spuler, S. M. and Fugal, J.: Design of an in-line, digital holographic imaging system for airborne measurement of clouds, Applied optics, 50, 1405–1412, 2011.

Steeneveld, G., Ronda, R., and Holtslag, A.: The challenge of forecasting the onset and development of radiation fog using mesoscale atmospheric models, Boundary-Layer Meteorology, 154, 265–289, 2015.

Tardif, R.: The impact of vertical resolution in the explicit numerical forecasting of radiation fog: A case study, in: Fog and Boundary Layer Clouds: Fog Visibility and Forecasting, pp. 1221–1240, Springer, 2007.

Thompson, B. J.: Holographic particle sizing techniques, Journal of Physics E: Scientific Instruments, 7, 781, 1974.

Touloupas, G., Lauber, A., Henneberger, J., Beck, A., Hofmann, T., and Lucchi, A.: A Convolutional Neural Network for Classifying Cloud Particles Recorded by Imaging Probes, Atmos. Meas. Tech. Discuss., 2019.

Touloupas, G., Lauber, A., Lucchi, A., Henneberger, J., Beck, A., and Hofmann, T.: A Convolutional Neural Network for Classifying Cloud Particles Recorded by Imaging Probes, Atmospheric Measurement Techniques, 2019 (submitted).

van der Linden, R., Fink, A. H., and Redl, R.: Satellite-based climatology of low-level continental clouds in southern West Africa during the summer monsoon season, Journal of Geophysical Research: Atmospheres, 120, 1186–1201, 2015.

Verlinde, J., Harrington, J. Y., McFarquhar, G., Yannuzzi, V., Avramov, A., Greenberg, S., Johnson, N., Zhang, G., Poellot, M., Mather, J. H., et al.: The mixed-phase Arctic cloud experiment, Bulletin of the American Meteorological Society, 88, 205–222, 2007.

Wanner, H. and Furger, M.: The bise—climatology of a regional wind north of the Alps, Meteorology and Atmospheric Physics, 43, 105–115, 1990.

Warren, G., Hahn, J., London, J., Chervin, M., and Jenne, L.: Global distribution of total cloud cover and cloud type amounts over land, 1986.

Warren, S. G., Hahn, C. J., London, J., Chervin, R. M., and Jenne, R. L.: Global distribution of total cloud cover and cloud type amounts over the ocean, Tech. rep., USDOE Office of Energy Research, Washington, DC (USA). Carbon Dioxide Research Div.; National Center for Atmospheric Research, Boulder, CO (USA), 1988.

Reviewer comments on '**Using a holographic imager on a tethered balloon system for microphysical observations of boundary layer clouds**' by Fabiola Ramelli, Alexander Beck, Jan Henneberger, Ulrike Lohmann

Response to Reviewer #1

We would like to thank the anonymous referee for his/her valuable feedback and suggestions on the paper. We incorporated the suggestions within the revised manuscript, which substantially improved the quality of the manuscript. In the following, we will address the comments and show the changes in the revised manuscript.

General comments

1) In this manuscript, the authors present a holographic imaging system and its application to the analysis of low stratus properties in a case study from Switzerland. The paper is well-written, has a clear structure, and overall presents a good overview of the potential of the technique in studying boundary-layer clouds. The case study presented includes some very interesting aspects, the resulting hypotheses are summarized in a useful conceptual sketch. Any generalization would require further samples, but is beyond the scope of this paper focused on the introduction of the technique.
2) Language: The paper is legible and understandable, but riddled with small lingual errors that could probably be corrected quickly by someone fully proficient in English

Detailed comments

1) **1-3: which cloud properties exactly?**
   Thank you for pointing this out. We have added the cloud properties as follows (page 1, line 6-7): "*Based on a set of two-dimensional images, information about the phase-resolved particle size distribution, shape and spatial distribution can be obtained."* More information about the cloud properties are provided in Sect. 1 and Sect. 3.1.

2) **1-4: since holographic imagers are not a common type of instrument in large parts of the cloud community, please add a very short note on the principle in the abstract**
   Thank you for pointing this out. We agree that holographic imagers are not a common type of instrument in large parts of the cloud community. We added a short description of the working principle in the abstract (page 1, line 4-8). Additionally, more information about the working principle of in-line holography can be found in Section 3.1.

3) **1-10: scales have been mentioned in line 7 already, but in contradiction to this line**
   Thank you for pointing this out. In the following study, only measurements down to the meter scale are presented. However, holographic imagers can provide information down to the millimeter scales if the spatial distribution of cloud particles is analyzed. The spatial

distribution of particles is not analyzed in the presented case study, but its potential is highlighted in Sect. 5.2.

4) **1-11: I think an example is not needed in the abstract**
   Thank you for the comment. The examples have been removed in the revised manuscript.

5) **2-10: What do you mean by "most of the observations", and how did you reach this conclusion?**
   Thank you for the comment. The term 'most' might be inadequate. We changed it accordingly to *'a large fraction of the observations'* (page 2, line 9). Moreover, we included some references, which used satellite observations to study boundary layer clouds.

6) **2-13: is there a source for this (problems in lowermost km)?**
   Thank you for pointing this out. We included two references describing the problem of surface clutter (page 2, line 14).

7) **2-21: what is "ice shattering", and how does it impact measurements?**

   Thank you for the comment. We included a short description of ice shattering and how it can impact the measurements (page 2, line 23-24): *"Ice shattering occurs if an ice crystal impacts the instrument tips or an inlet prior to entering the detection volume, which can result in a large number of small ice particles being a measurement artefact."*

8) **3-3: some additional info on the principles of holography would be useful here**
   Thank you for the comment. We add a reference to Section 3 (page 3, line 11), where a more detailed description of the holographic instrument and holography is provided.

9) **3-18: i.e. a low stratus cloud with its cloud base above ground? Please specify.**
   Thank you for pointing this out. We removed the term high fog throughout the whole paper and replaced it by stratus clouds, which is the more general term. The term 'high fog' is mainly used in Switzerland and therefore introduced at the beginning of the case study (page 10, line 2).

10) **3-20: how do you define inhomogeneity here?**

    Thank you for the comment. We added a definition of inhomogeneity (page 3, line 30-31): *"Throughout this study, inhomogeneities are defined by the variability in the cloud droplet number concentration and cloud droplet size."*

11) **5-27: What do you use as training data?**
12) **5-28: How are these parameters calculated?**
13) **5-28: "such as" – please be specific here and list all parameters.**

Thank you for the comments. The comments 11-13 are addressed together. In order to provide more details about the particle classification, we extended the description as follows (page 5, line 27-33): "*The resulting 2D shadowgraphs can be classified as cloud droplets, ice crystals and artefacts based on a set of parameters using supervised machine learning (e.g. Fugal et al. 2009, Beck et al. 2017, Touloupas et al. 2019). In the present study, a set of 6400 particles was classified manually, which served as a training data set on support vector machines. From the classification, the phase-resolved particle size distribution can be computed. The particle diameter is calculated based on the number of pixels (see also Sect. 3.3) and the number concentration can be computed from the particle counts within the well-defined sample volume. Only particles that exceed a size of 2x2 pixels (6 µm) are considered.*"

14) **9-5: Why was this particular situation chosen? In what ways is it representative or not?**

Thank you for the comment. The presented stratus cloud event is representative for a Bise situation, which often occurs during winter (page 10, line 3-4). Below, we added a figure from Wanner and Furger (1990), which summarizes the frequency of wind direction from radiosonde ascents launched from Payerne for the period 1981-1985. Based on their result, Bise occurred on 27% of the hours (see also Weber and Furger, 2001 or MeteoSwiss).

Wanner, H., & Furger, M. (1990). The bise—climatology of a regional wind north of the Alps. *Meteorology and Atmospheric Physics*, 43(1-4), 105-115.

Weber, R. O., & Furger, M. (2001). Climatology of near-surface wind patterns over Switzerland. *International Journal of Climatology: A Journal of the Royal Meteorological Society*, *21*(7), 809-827.

MeteoSwiss:https://www.meteoschweiz.admin.ch/content/dam/meteoswiss/de/service-und-publikationen/Publikationen/doc/Web_Wetterlagen_DE_low.pdf

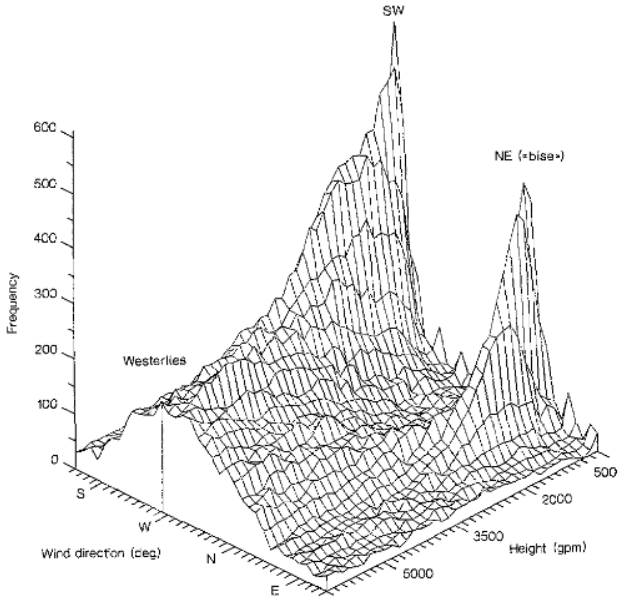

Fig. 4. Frequency of wind directions for 150 m layers from 500 to 6 200 m ASL for radiosonde ascents from Payerne for the period 1981–1985

15) Figure 5: Please provide complete citation (author, year)

Thank you for the comment. We added the year and the link where the online maps can be downloaded (https://www.atlasderschweiz.ch/) (caption Fig. 5).

16) Table 2: Why is there no descent for profile number 9?

Thank you for the comment. There is no profile 10/ no descent for profile number 9, because the battery of the instrument package was empty. We added a sentence to specify that (page 11, line 18-19): *"The battery of the instrument package was empty after profile 9, thus no observations were available afterwards."*

17) 11-18: What do you mean by classification in this context? Which classes?

18) 11-18: How is a classification by hand performed?

Thank you for the comments. The particles are classified into three classes (cloud droplets, ice crystals and artefacts). We added the classes in the text and added a reference to Sect. 3.1 (page 12, line 4), where the classification process is described in more detail. Moreover, we exchanged the term 'classification by hand' with the term *'classified manually (visual classification)'* (page 12, line 5).

19) Section 4.3: How do you explain the nearly constant with height droplet diameters?

Thank you for pointing this out. Figure 7.c) shows the mean vertical profile of the cloud droplet diameter. We agree that in the mean, the cloud droplet diameter looks rather constant. Here we include a figure that shows the individual vertical profiles of the cloud droplet diameter. It can be seen that in general the mean cloud droplet diameter increases with height. Profile 7 shows a lower mean diameter than the other profiles at altitudes above 1050 m.

Furthermore, it is also possible that there is a higher competition for water vapor with increasing height due to the increasing CDNC.

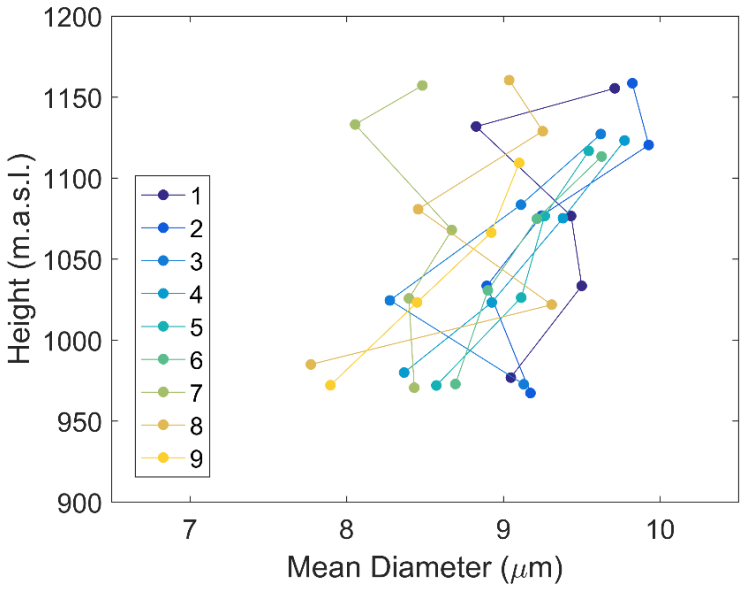

20) **17-12: I think this statement is too general, given that only one case is analyzed.**
Thank you for the comment. We agree that this statement is too general, since the analysis is based on the observations of only one case study. We adapted the sentence in the following way (page 18, line 19-20): "*We found that stratus clouds can exhibit complex dynamic structures with microphysical signatures on different scales (Sect. 4.4).*"

Technicalities

Thank you for all the technical comments

1) page 1, line 1 (henceforth 1-1 etc.): aircrafts→aircraft
Changed to aircraft (page 1, line 1)
2) 1-2: orographically diverse
Changed (page 1, line 2)
3) 1-2: densely populated
Changed (page 1, line 2)
4) 1-5: velocity-independent sample
Changed (page 1, line 7)
5) 1-6: allows for observations
Changed (page 1, line 9)
6) 1-7: scales
We think that 'scale' should be used in singular in this case.
7) 1-9: above the ground were performed at temperatures...
Changed (page 1, line 13)
8) 1-11: scales (No more comments on language from this point forward)
We think that 'scale' should be used in singular in this case.

Reviewer comments on '**Using a holographic imager on a tethered balloon system for microphysical observations of boundary layer clouds**' by Fabiola Ramelli, Alexander Beck, Jan Henneberger, Ulrike Lohmann

Response to Reviewer #2

We would like to thank the anonymous referee for his/her valuable feedback and suggestions on the manuscript. We incorporated the suggestions within the revised manuscript, which substantially improved the quality of the manuscript. In the following, we will address the comments.

General comments

The paper describes balloon-borne measurements of microphysics inside supercooled boundary layer stratus clouds collected with use of a modern holographic imager HOLIMO. The paper consists of two very distinct parts. From the beginning to section 4.3 the paper is clear, very well written and there are no major drawbacks in the text. The description of the measurements, calibration is sound. The results are interesting, show unexpected behavior of cloud microphysics, hard to document with different, than HOLIMO instruments. This, with some additional discussion and maybe selected examples of local samples of droplet spatial and size distributions would be enough to justify the publication. However, instead of focusing on microphysics, in the last sections of chapter 4 and in the discussion author speculate on mixing and dynamical effects which are aimed at explanation the unexpected results of microphysical measurements, in particular large variations in droplet number concentration. These speculations should be backed with the data, but are not. As shown in Fig.1 the HoloBallon is, together with the HOLIMO, equipped with a sonic anemometer, which should provide in-situ high-resolution data on turbulence (velocity fluctuations) and virtual temperature. The authors, instead of using data from the device, speculate on turbulence and waves, Kelvin-Helmholz Instabilities, downdrafts. I strongly believe that insight into sonic data could be used to verify which speculations are justified and which are not. In particular virtual temperature fluctuations might help to understand mixing, velocity records should allow to document turbulence, waves and K-H instabilities.

In my opinion the paper in the present form is hardly acceptable. I suggest the major revision of the text. Two options is possible: 1) to make the paper shorter, remove the speculative part of the chapters 4 and 5 and to write that the explanation requires additional, highly demanding analysis of turbulence data recorded; 2) to use sonic data and do the analysis in a simplified form, to show some dynamical properties of the flow to support speculations presented in the text.

If the authors chose the second option, I suggest more detailed insight into the cited Mellado's paper about stratocumulus top and into references therein. Such insight, in my opinion, could help very much in the analysis.

Thank you very much for your valuable comments and suggestions. In the substantially revised manuscript (especially Sect. 4.4 and Sect. 5), we focus more on the technical aspects of the HoloBalloon platform, rather than on the scientific outcome of Sect. 4.4. We agree that further data and analysis are required to back the hypotheses presented in Sect. 4.4. As the aim of the paper is (1) to introduce and characterize the newly developed HoloBalloon platform, (2) to provide a proof of concept for the HoloBalloon platform (case study) and (3) to show the potential and limitations of the platform in studying boundary layer clouds, we shortened the section 4.4 (especially the speculative part) as well as the discussion of it. Furthermore, we clearly indicate that further analysis of our data as well as auxiliary data (e.g. three-dimensional wind field, turbulence) are required to study the proposed mechanisms/ test the hypotheses, which lies beyond the scope of this paper.

We agree that the data of the 3D sonic anemometer could provide useful information about the dynamical properties of the flow and help to support the proposed hypotheses. However, we decided to not analyze the turbulence data of the 3D sonic anemometer, as it is installed on the keel below the balloon. Several experts in the field advised us to install the instrument package in future 20-30 m below the balloon in order to reduce influences of the balloon on the turbulence measurements. Thus, in the present study we cannot exclude influences of the balloon on the turbulence measurements (described in Sect. 5.1). For future field campaigns, we will follow the advices and install the instrument package 20-30 m below the balloon to be able to analyze turbulence data of the 3D sonic anemometer. The feasibility of a hanging mount was already successfully tested in the field in autumn 2019.

In the revised manuscript, we changed the order of subsections 5.1 and 5.2 in the discussion section. Moreover, we completely rewrote Sect. 5.2 (previous 5.1). In Sect. 5.2, we focus more on the technical aspect of HoloBalloon, rather than on the scientific outcome of Sect. 4.4 (in contrast to the previous version). The observations of the presented case study are used as an example to discuss the potentials and limitations of the HoloBalloon in studying boundary layer clouds.